- 1 Detecting hydrologic distinctions among Andean lakes using clumped and triple oxygen
- 2 isotopes

3

- 4 **Authors:** Sarah A. Katz^{1*}, Naomi E. Levin¹, Donald T. Rodbell², David P. Gillikin², Phoebe G.
- 5 Aron¹, Benjamin H. Passey¹, Pedro M. Tapia³, Analucía R. Serrepe⁴, and Mark B. Abbott⁵

6

- ¹Department of Earth and Environmental Sciences, 1100 North University Ave, University of
- 8 Michigan, Ann Arbor, MI, 48109, USA
- ²Geosciences Department, 807 Union Street, Union College, Schenectady, NY, 12308, USA
- ³Instituto Nacional de Investigación en Glaciares y Ecosistemas de Montañas, Huaraz, Ancash,
- 11 Perú
- ⁴Ciencias del Mar, Universidad Peruana Cayetano Heredia, Lima, Perú
- ⁵Department of Geology and Environmental Science, University of Pittsburgh, PA,
- 14 15260, USA

15

16

*Correspondence to: skatzees@umich.edu

17

18

Highlights:

- Expansion of lake water and carbonate Δ'^{17} O observations to humid systems
- Carbonate Δ_{47} and Δ'^{17} O track lake water temperature and isotopic composition
- $\Delta'^{17}O$ can track the evaporative state of lakes (X_E) in both humid and arid regions
- Refined $\Delta'^{17}O$ - λ_{lake} relationship improves $\delta^{18}O_{rucp}$ estimates in humid systems
- Even in the absence of humidity constraints, $\Delta'^{17}O$ data improve $\delta^{18}O_{\text{rucp}}$ estimates

Abstract:

24

25

26

27

28

29

30

31

32

33

34

35

36

37

38

39

40

41

42

43

44

45

46

Oxygen isotope distributions from lacustrine carbonates provide insights into climate and hydrological change, but it is difficult to isolate the influences of catchment precipitation δ^{18} O, water temperature, and evaporation on lacustrine carbonate δ^{18} O values. Recent work shows the potential for using a combination of clumped (Δ_{47}) and triple oxygen isotope (Δ'^{17} O) measurements to identify the roles of temperature and evaporation on carbonate δ^{18} O values in lakes, allowing precipitation δ^{18} O values to be inferred and facilitating paleoclimate reconstructions. However, modern calibration of this approach has been mostly limited to arid regions with a high ratio of evaporative losses over inputs (X_E) and low relative humidity (h <0.7). Developing this tool for paleoclimate and paleoelevation reconstructions requires expanding the modern calibrations to a greater range of climatic and hydrologic conditions. We sampled four lakes in different hydrologic states under a single, high humidity climate regime (h= 0.7–0.9) in the Lake Junín region of central Peru. Clumped isotope temperatures from lake carbonates reflect water temperatures during carbonate formation. Lake hydrology is the main control on the Δ'^{17} O values of carbonates and waters: Δ'^{17} O values are lowest in the larger lakes with higher X_E when compared to smaller, headwater lakes where evaporation is minimal and Δ'^{17} O is indistinguishable from that of precipitation. Reconstructed unevaporated catchment precipitation $\delta'^{18}O(\delta'^{18}O_{\text{rucp}})$ values from lake waters relies on accurate characterization of λ_{lake} , the triple oxygen isotope evaporation slope. We explore the influence of humidity on λ_{lake} using both new observations and modeled data. Accounting for local humidity improves λ_{lake} estimates, which allows for more accurate reconstructions of $\delta'^{18}O_{rucp}$. We generate a $\delta'^{18}O_{rucp}$ value of -15.2 ±2.1% from modern carbonates and waters (n= 15) in the Lake Junín region, which is similar to amount weighted mean annual precipitation -14.1 (±2.2%). This study

illustrates that (1) $\Delta'^{17}O$ can be used to differentiate between lakes with differing X_E in humid climates, (2) lake carbonate $\Delta'^{17}O$ and $\delta^{18}O$ values can be used to evaluate the influence of evaporation on lake water $\delta^{18}O$ values in a range of climates, and (3) modeling λ_{lake} under appropriate humidity conditions improves $\delta'^{18}O_{rucp}$ estimates from lake carbonate $\Delta'^{17}O$.

51

52

- 53 **Keywords**: triple oxygen isotopes, clumped isotopes, evaporation, lake carbonates, Andes, Lake
- 54 Junín

1. Introduction:

55

56

57

58

59

60

61

62

63

64

65

66

67

68

69

70

71

72

73

74

75

76

77

Lakes are sensitive to changes in atmospheric processes, hydrology, and climate such that lake sediments are commonly used to reconstruct past climate (Seltzer et al., 2000; Leng and Marshall, 2004; Bird et al., 2011a). Stable oxygen isotope distributions in lake carbonates are powerful paleoclimate archives because they record information about $\delta^{18}O$ values of precipitation, water temperature, and evaporation (Figure 1; Leng and Marshall, 2004). However, difficulty isolating the controls on lake carbonate $\delta^{18}O$ limits their efficacy in paleoclimate and paleoelevation studies (Seltzer et al., 2000; Horton et al., 2016). Recent studies address these limitations and expand the utility of lake carbonates by using clumped and triple oxygen isotopes to constrain temperature and evaporative fluxes (e.g., Huntington et al., 2015; Passey and Ji, 2019). Advances in clumped isotope carbonate thermometry provide constraints on both the temperature and δ^{18} O values of ancient lake water (e.g., Huntington et al., 2010, 2015; Hren and Sheldon, 2012; Petryshyn et al., 2015; Horton et al., 2016). However, even with these constraints, forming interpretations about hydrology, climate, or elevation from δ^{18} O values of reconstructed formation waters ($\delta^{18}O_{rfw}$), is difficult without knowing the evaporation state of the water and its relationship to the isotopic composition of precipitation (e.g., Horton et al., 2016). High-precision triple oxygen isotope geochemistry offers a new approach for identifying the role of evaporation in lake budgets and for stripping away evaporative effects on $\delta^{18}O_{rfw}$ values (Luz and Barkan, 2010; Passey et al., 2014; Gázquez et al., 2018; Surma et al., 2018; Passey and Ji, 2019). These studies use the Δ'^{17} O parameter, which represents the deviation from a reference line (λ_{ref}) in δ'^{18} O and δ'^{17} O space ($\lambda_{ref} = 0.528$; where δ'^{x} O=ln(δ^{x} O+1); Figure 1; e.g., Luz and Barkan, 2010). Evaporation involves both equilibrium and kinetic fractionations, resulting in

residual waters with low $\Delta'^{17}O$ values, as kinetic processes follow a shallower slope than λ_{ref} (Barkan and Luz, 2005; Luz and Barkan, 2010). The magnitude of kinetic fractionation during evaporation partially depends on local humidity (Landais et al., 2006), thereby linking humidity and the evaporation slope: λ_{lake} .

Combining measurements of carbonate $\Delta'^{17}O$ and clumped isotope derived temperatures allows formation water $\Delta'^{17}O$ values ($\Delta'^{17}O_{rfw}$) to be calculated and used towards evaluating evaporative losses from lakes, (i.e., X_E the fractional loss of evaporation relative to inflowing waters; Herwartz et al., 2017; Gázquez et al., 2018; Passey and Ji, 2019). As Passey and Ji (2019) illustrate, $\Delta'^{17}O_{rfw}$ and $\delta^{18}O_{rfw}$ are related to $\Delta'^{17}O$ and $\delta^{18}O$ of unevaporated precipitation by the evaporation slope, λ_{lake} , such that $\delta^{18}O$ of unevaporated catchment precipitation ($\delta^{18}O_{ruep}$) can be reconstructed via "back projection" (Figure 1). Recently, the back projection approach has been applied to Eocene cherts (Ibarra et al., 2021) and bivalves (Kelson et al., 2022). This approach depends on knowledge of λ_{lake} , which has been studied in closed-basin lakes and arid environments (Surma et al., 2018; Passey and Ji, 2019) and a temperate lake (Pierchala et al., 2022), but we are not aware of a study that explores the role of humidity on λ_{lake} nor that study lakes with varying X_E within humid settings.

Here we present a dataset of the triple oxygen isotope compositions of precipitation, surface waters, and lacustrine carbonates from four lakes with different hydrological configurations in the central Peruvian Andes where relative humidity is >0.7 (Table S1; SENAMHI, 2022). Our data contribute to clumped isotope datasets of modern lake carbonates and fill a data gap for $\Delta'^{17}O$ and λ_{lake} from low X_E lakes in humid settings. We evaluate these data by modeling expected distributions under steady state conditions for lake water evaporation, which enables us to refine the relationship between $\Delta'^{17}O$ and λ_{lake} for humid climates.

101

102

103

2. Isotope Notation

2.1 Oxygen and hydrogen isotopes

Isotope fractionation is described by a fractionation factor, α, where R_A and R_B represent the ratio of heavy to light isotopes of two phases or materials:

$$\alpha_{A-B} = \frac{R_A}{R_B}$$

$$107 (1)$$

In the triple oxygen isotope system, 18 O, 17 O, 16 O, a power law describes mass-dependent relationships between $^{18}\alpha_{A-B}$ and $^{17}\alpha_{A-B}$, which are related by a fractionation exponent, θ (Young et al., 2002):

$$^{17}\alpha_{A-B} = \left(^{18}\alpha_{A-B}\right)^{\theta}$$

$$112 (2)$$

We also use the term λ , which is mathematically equivalent to θ , for "apparent"

fractionation exponents that represent a combination of multiple fractionation processes.

115 Conventionally, isotope ratios are reported in "delta notation":

$$\delta = \left(\frac{R_A}{R_{\text{standard}}} - 1\right)$$

$$117 (3)$$

However, isotope ratios may also be expressed in logarithmic form (Hulston and Thode,

119 1965):

$$\delta' = \ln\left(\frac{R_A}{R_{standard}}\right)$$

$$121 (4)$$

This "delta prime" notation is commonly used in triple oxygen isotope studies (see Miller and Pack, 2021, and references therein). In a triple oxygen isotope plot, i.e., $\delta'^{18}\text{O-}\delta'^{17}\text{O}$,

deviations from a reference line (Figure 1C) are quantified using the expression for $\Delta'^{17}O$:

125
$$\Delta'^{17}0 = \delta'^{17}0 - \lambda_{\text{ref}} \times \delta'^{18}0$$

$$126 (5)$$

Frequently, $\Delta'^{17}O$ is reported in units of "per meg." The reference slope, λ_{ref} , is

commonly defined as 0.528 in hydrological studies (Luz and Barkan, 2010; Aron et al., 2021a)

and we follow this convention. The $\Delta'^{17}O$ term is analogous to d-excess in $\delta^{18}O$ - δ^2H space

 $d-excess = \delta^2 H - 8 \times \delta^{18} O$

133

134

135

136

137

138

139

140

141

130

2.2. Carbonate clumped isotopes

(Figure 1A,B; Dansgaard, 1964):

The abundance of multiply substituted or "clumped" isotopologues relative to a stochastic baseline is temperature-dependent in carbonates (Schauble et al., 2006; Eiler, 2007, 2011). In CO₂ derived from acid digestion of carbonates, m/z 47 is the most abundant clumped isotopologue. The enrichment of $^{13}C^{-18}O$ bonds in carbonate minerals is calculated based on simultaneous collection of m/z 44–49 during analysis (which inherently yields sample $^{13}C/^{12}C$ and $^{18}O/^{16}O$) and is defined as Δ_{47} , where R and R* values represent measured and stochastic isotope ratios, respectively, compared to m/z 44 (Wang et al., 2004; Eiler, 2011):

142
$$\Delta_{47} = \left[\left(\frac{R47}{R47^*} - 1 \right) - \left(\frac{R46}{R46^*} - 1 \right) - \left(\frac{R45}{R45^*} - 1 \right) \right] \times 1000$$

$$143 (7)$$

 Δ_{47} values have an inverse relationship to temperature (Schauble et al., 2006; Eiler, 2007, 2011) as documented theoretically and empirically in carbonate materials (e.g., Wang et al., 2004; Petersen et al., 2019), such that it is becoming a widespread approach for determining carbonate formation temperatures. We use the term $T_{\Delta 47}$ to represent reconstructed carbonate formation temperatures derived from clumped isotopes. $T_{\Delta 47}$ can be used to calculate formation water values ($\delta^{18}O_{rfw}$) from carbonate $\delta^{18}O$ assuming equilibrium growth conditions (Kim and O'Neil, 1997).

3. Study Area and Materials:

3.1 Study area:

The Lake Junín region in central Peru is an intermontane plateau between the Andean Cordilleras (4000–4600 m above sea level; Figure 2; Table 1). Mean annual air temperature (MAT) is 6.5°C and annual precipitation is 900–1000 mm, with approximately 70% of rainfall from October–April (Table S1; SENAMHI, 2022). Mean annual potential evapotranspiration is 525–550 mm/year. Relative humidity is between 70–90% year-round, rarely falling below 70% (SENAMHI, 2022). Relative humidity normalized to lake surface temperature is >70%.

Glaciation of the Lake Junín region has resulted in many lakes that exist under the same climatic conditions but differ in size and hydrology. Jurassic–Triassic aged limestone bedrock of the Pucarà Group leads to high bicarbonate concentrations in local surface waters and production of authigenic carbonate in many lakes (Cobbing et al., 1996; Flusche et al., 2005).

We sampled two small lakes and two larger lakes (lake surface area <10 km² and >10¹– 10² km², respectively; Figure 2; Table 1). The smaller lakes, Pumacocha and Mehcocha, are headwater lakes in glacial valleys and have continuous inflow and outflow. Pumacocha's

maximum water depth is 23.5 m, whereas at Mehcocha it is 25.5 m in the upper basin and 12.4 m in the lower basin (Bird et al., 2011b). We estimate that X_E for Pumacocha and Mehcocha is very low (X_E <0.1) and characterize them as "unevaporated," consistent with a short residence time for small, continuously overflowing lakes (e.g., Bird et al., 2011b, 2011a). The other lakes, Yanacocha and Lake Junín, have much larger watersheds. Yanacocha sits in a glacial valley with sub-basins that result in a larger lake surface area and more complex hydrology than the smaller lake systems (Figure 2B). Lake Junín is the largest of the four lakes sampled and sits in a fault-bounded basin, surrounded by alluvial fans. It is the second largest lake in Peru by surface area (~300 km²), but it is shallow with a maximum water depth of 15 m (Figure 2B; Seltzer et al., 2000). Currently, a 4 m high dam situated downstream from the inflow/outflow regulates water level, which impacts hydrology by increasing wet season inflow and dry season outflow. We expect annual variations in X_E may be low, however we lack quantitative X_E estimates.

3.2 Sample Collection:

3.2.1 Waters: To monitor precipitation, we installed a Palmex[™] rain gauge in the town of Junín (Figure 2). From June 2016–June 2018 monthly samples were collected by local citizens and stored in sealed 50 mL Falcon tubes (Corning #352070). Surface waters were collected in May 2016, 2017, and 2019 from various water types, including springs, streams, rivers, lakes, and isolated pools. Sampling locations are reported in Tables S1-S2.

3.2.2 Carbonates: In May 2019 we collected nine shallow, nearshore sediment samples, one sample from deeper, open water at Mehcocha using an Ekman box sampler, and one sample from carbonate rinds on cobbles in Pumacocha's outflow stream (Figure 2; Table 2).

Stratigraphy was not preserved during collection, so bulk sediment samples represent the upper ~ 10 cm of the sediment-water interface. Exploring the effects of lake hydrology on carbonate Δ_{47} and Δ'^{17} O values motivated our sampling at different lakes. Given the remote field location and COVID-19 pandemic we were unable to collect additional samples. Long-term monitoring and sampling of microenvironments within lakes are logical next steps to refine Δ_{47} and Δ'^{17} O calibration studies.

We processed bulk lake sediments to concentrate authigenic carbonate by reacting samples overnight with 7% hydrogen peroxide to remove organics and wet sieving through a 63 μ m mesh, retaining the <63 μ m size fraction. The processed samples appear homogenous, light in color, and devoid of macroscopic shells. All geochemical analyses of lake carbonates were conducted on the <63 μ m size fraction.

We collected local bedrock (Table 2) to characterize limestone Δ_{47} and evaluate detrital contamination in lake carbonate samples. Samples were powdered with a DremelTM drill from fresh-cut, interior surfaces to avoid weathering surfaces.

4. Analytical Methods and Data Standardization:

4.1 X-ray diffraction:

Lake sediments and bedrock samples were analyzed on a Rigaku Ultima IV X-ray diffractometer at the University of Michigan (UM) Electron Microbeam Analysis Lab over a 15–65° angle of incidence (Table S3). Spectral data were corrected for background noise and normalized by relative peak intensity.

4.2 Isotopic measurements:

4.2.1 δ^8O and δ^2H : Waters collected in 2016 and 2017 were analyzed at Union College on a ThermoScientific Gas Bench II ($\delta^{18}O$) and TC/EA (δ^2H) peripherals coupled to a Delta V Advantage mass spectrometer in continuous flow mode. Analytical precision was 0.02% for $\delta^{18}O$ and 1.0% for δ^2H based on in-run analyses of calibrated internal lab standards.

Water samples collected in 2017 and 2019 were analyzed at UM via Cavity Ring Down Spectroscopy (Picarro model L2130-i analyzer with high precision vaporizer (A0211)). Sample data were corrected using ChemCorrectTM software and standardized to the VSMOW-SLAP scale using USGS reference waters (USGS 45–47,50) and four calibrated in-house standards. Long-term instrument precision is better than 0.1% for δ^{18} O and 0.3% for δ^{2} H.

Waters analyzed at both institutions were within the combined $\delta^{18}O$ and $\delta^{2}H$ uncertainty range for 94% of samples, suggesting excellent inter-laboratory agreement (Table S2).

4.2.2 Triple oxygen isotopes: Triple oxygen analyses were conducted at the UM Isotopologue Paleosciences Lab (IPL, Tables S4-S7). For carbonates, we use a three step process to convert CaCO₃ to an O₂ analyte following the methods of Passey et al. (2014): 1) CaCO₃ is digested in >100 wt% H₃PO₄ at 90°C to liberate CO₂; 2) the CO₂ is passed through a circulating loop over an Fe catalyst at 560°C in the presence of H₂ gas to transfer oxygen from the CO₂ to H₂O; 3) the H₂O is then reacted with cobalt trifluoride (CoF₃) at 360°C to produce O₂. After passing through a series of GC columns and cryogenic traps, the purified O₂ is transferred to a Nu Perspective isotope ratio mass spectrometer where measurements of m/z 32–36 are made in dual inlet mode on sample and reference gases. For waters, steps 1) and 2) are bypassed and samples are injected directly into the same fluorination line as used for carbonates. The UM IPL

fluorination line and mass spectrometer configuration was recently described in detail by Aron et al. (2021a), thus is not discussed further here.

Triple oxygen data are standardized to the VSMOW-SLAP scale where $\delta^{18}\text{O}_{\text{VSMOW}}=$ 0.000%, $\delta^{17}\text{O}_{\text{VSMOW}}=$ 0.000%, $\delta^{18}\text{O}_{\text{SLAP2}}=$ -55.500%, and $\delta^{17}\text{O}_{\text{SLAP2}}=$ -29.6986% (Schoenemann et al., 2013) via multiple analyses of both VSMOW2 and SLAP2 during every analytical session. Water $\delta'^{18}\text{O}$, $\delta'^{17}\text{O}$, and $\Delta'^{17}\text{O}$ precision is 0.5%, 0.3%, and 9 per meg, respectively, based on the pooled standard deviation of USGS water standards run concurrently with our samples (Tables S8-S9). We normalize carbonate data to the mineral $\Delta'^{17}\text{O}$ values for IAEA-C1 reported by Wostbrock et al. (2020b) and applied a linear drift correction based on NBS19 $\Delta'^{17}\text{O}$ residuals (following Huth et al., 2022). Carbonate $\delta'^{18}\text{O}$, $\delta'^{17}\text{O}$, and $\Delta'^{17}\text{O}$ precision is 1.0%, 0.5%, and 7 per meg, respectively, based on the pooled standard deviation of carbonate standards run concurrently with our samples (Tables S8-S9).

4.2.3 Clumped isotopes: Carbonates were digested in a common acid bath (>100 wt% H₃PO₄) at 90°C following methods outlined by Passey et al. (2010). Liberated CO₂ was purified using a series of cryotraps and a GC column prior to analysis on a Nu Perspective mass spectrometer in dual inlet mode at the UM IPL. Δ_{47} values are reported (Table S10) relative to the carbon dioxide equilibrium scale of Dennis et al., (2011) via multiple analyses of 'heated gases' (CO₂ gases of differing δ¹³C and δ¹⁸O compositions heated at 1000°C for >2 hours offline) and 'equilibrated gases' (as above, but equilibrated with water at 30°C). ¹⁷O–corrections were made using 'Brand parameters' (e.g., Petersen et al., 2019). A moving gas line scheme is used to account for temporal drift in linearity and scale compression (Passey et al., 2010). Δ_{47}

analytical precision on this system is $\pm 0.021\%$, based on the long-term pooled standard deviation of carbonate standards (Table S9).

5. Results:

5.1 X-ray diffraction:

Lake carbonates (n= 5) and bedrock (n= 3) are entirely calcite based on comparison with carbonate reference spectra (Figure S1; Table S3).

5.2 Isotope results:

5.2.1 Precipitation:

Junín precipitation δ^{18} O and δ^{2} H values range from -20.9‰ to -4.8‰ and -158.2‰ to -17.8‰, respectively (n= 21; Figure 3; Table S1). A subset of samples were also analyzed for triple oxygen isotopes (Δ'^{17} O= 12–43 per meg; n= 5; Tables 3.S1).

We screen precipitation samples for data quality and assume samples with identical isotope values (i.e., <0.5‰ variation in δ^{18} O for consecutive months) do not reflect precipitation. These may reflect groundwater or tap sources, as also observed in other studies that employ citizen scientists (e.g., Aron et al., 2021b). Based on this criterion, we identify seven samples from the Junín dataset (Oct. 2017–April 2018) with identical isotope values; these data are included in Table S1 but excluded from figures and calculations.

Local meteoric water lines at Junín are: $\delta^2 H=8.61(\pm 0.08) \times \delta^{18} O+21.9(\pm 1.1)$ (n= 13) and $\delta'^{17} O=0.5282(\pm 0.0010) \times \delta'^{18} O+0.0333(\pm 0.0170)$ (n= 5, Table S11). We calculated the weighted mean isotopic composition of precipitation at Junín, hereafter referred to as "amount-weighted annual precipitation." Weightings assume the same monthly rainfall amounts in 2016 and 2017

(gauge installation at Junín occurred in 2017) and are consistent with seasonal rainfall amount patterns observed regionally (Table S1) (SENAMHI, 2022). Amount-weighted annual precipitation δ^{18} O, δ^{2} H, d-excess, and Δ'^{17} O values are -14.1‰ (±2.2‰), -100.3‰ (±18.7‰), 12.8‰ (±1.3‰), and 31 per meg (±5 per meg) respectively, where uncertainty is the standard error of the weighted mean.

5.2.2 Surface waters:

Surface water δ^{18} O, δ^{2} H, and d-excess values range from -16.9 to 1.5‰, -126.1 to -23.3‰, and -35.3 to 13.5‰, respectively (Figure 3; Table S2). Surface water Δ'^{17} O values range from -28 to 36 per meg (n= 16; Figures 3–4; Tables 3,S2).

Lake waters from the smaller lakes (Pumacocha, Mehcocha), springs, and rivers are isotopically similar to local precipitation while waters from larger lakes have lower $\Delta'^{17}O$ and d-excess than precipitation (Yanacocha, Lake Junín; Figures 3,4). In the larger watersheds, we observe variability in the isotopic composition of waters and isotopic trends based on position within the catchment (similar to a "chain of lakes" scenario); inflow waters have lower $\delta^{18}O$, $\delta^{17}O$, and $\delta^{2}H$, and higher $\Delta'^{17}O$ and d-excess values than downstream lake waters and outflow streams (Figures 3,4). Despite hydrologic modifications, the Lake Junín system follows these trends.

Considering all surface waters from the Lake Junı́n region together, they follow linear distributions in $\delta^{18}\text{O}-\delta^2\text{H}$ and $\delta'^{18}\text{O}-\delta'^{17}\text{O}$ space with lower slopes than those observed from precipitation. Regressions of surface water $\delta^{18}\text{O}-\delta^2\text{H}$ and $\delta'^{18}\text{O}-\delta'^{17}\text{O}$ yield evaporation lines: $\delta^2\text{H}=5.39(\pm0.06)\times\delta^{18}\text{O}-32.73(\pm0.82)$ and $\delta'^{17}\text{O}=0.5248(\pm0.0004)\times\delta'^{18}\text{O}-0.0208(\pm0.0044)$ (Table S11). We determined empirical triple oxygen isotope evaporation slopes,

 $\lambda_{lake} = \delta'^{17} O_{lake} - \delta'^{17} O_{precip} / \delta'^{18} O_{lake} - \delta'^{18} O_{precip}, \ using the amount-weighted isotopic composition of precipitation (Table S12). At Lake Junín the range in observed <math display="inline">\lambda_{lake}$ is 0.523–0.525. At Yanacocha, observed λ_{lake} ranges from 0.525 in the upper lake to 0.522 at its outlet. We did not calculate evaporation slopes for the smaller lakes, Mehcocha and Pumacocha, given the similar isotopic composition of lake water and amount-weighted annual precipitation.

5.2.3 Carbonates:

We report $\delta^{18}O$, $\delta^{17}O$, $\delta^{13}C$, and Δ_{47} data for lacustrine and bedrock carbonates in Tables 2, S7, S10. Carbonate $\delta^{18}O$ and $\delta^{13}C$ values generated during Δ_{47} analysis range from 17.2 to 21.3% (VSMOW) and -3.7 to 0.1% (VPDB) for lacustrine carbonates and 23.5 to 25.3% (VSMOW) and -2.3 to 1.3% (VPBD) for bedrock, respectively (Table 2). Using Δ_{47} values, we calculate carbonate formation temperatures, $T_{\Delta 47}$, which are 13 $\pm 3^{\circ}C$ (n= 8) and 61 $\pm 4^{\circ}C$ (n= 3) for lacustrine and bedrock carbonates respectively (Figures

 $\pm 3^{\circ}$ C (n= 8) and 61 $\pm 4^{\circ}$ C (n= 3) for lacustrine and bedrock carbonates respectively (Figures 5,S3; Table 3; Bonifacie et al., 2017). We assume equilibrium growth conditions and use the temperature-dependent equilibrium fractionation factor ($^{18}\alpha_{calcite-water}$) and $T_{\Delta47}$ to calculate reconstructed formation water δ^{18} O values (δ^{18} O_{rfw}; Table 2; Figure 5C; Kim and O'Neil, 1997). Uncertainties on $T_{\Delta47}$ and δ^{18} O_{rfw} values were determined using a Monte Carlo re-sampling approach. We assume a Gaussian distribution for carbonate δ^{18} O and Δ_{47} values among sample replicates and in the slope and intercept values of the temperature-dependent transfer function (Kim and O'Neil, 1997). Unique combinations of $T_{\Delta47}$ and δ^{18} O_{rfw} values were generated (n= 10,000), from which we report the mean and 1σ standard deviation (Table S3, Supplemental Script 1).

The triple oxygen isotope composition of lacustrine carbonates, Δ'^{17} O, range from -90 to -67 per meg (VSMOW-SLAP; Tables 2,S7). Formation water $\delta'^{18}O_{rfw}$ and $\Delta'^{17}O_{rfw}$ values calculated from δ^{18} O, Δ'^{17} O, δ^{18} O, δ'^{18} O, δ'^{18} O, and 1 to 28 per meg (VSMOW-SLAP, Tables 2,S13, Figures 4,5D). To determine Δ'^{17} O_{rfw}, we use an equilibrium $\lambda_{\text{calcite-water}}$ value of 0.5250 (± 0.0002), generated from synthetic carbonates in our lab (UM IPL) (Huth et al., 2022); this is indistinguishable to a value of 0.5249 (± 0.0002) from modern bivalves also generated in our lab (Kelson et al., 2022) and is consistent with $\lambda_{\text{calcite-water}}$ values from natural and synthetic carbonates (0.5241–0.5250) compiled by Huth et al. (2022). We are not aware of any $\lambda_{\text{calcite-water}}$ values generated specifically for lacustrine carbonates. Our selected $\lambda_{\text{calcite-water}}$ is lower than some theoretical calculations (0.5253–0.5256; Guo and Zhou, 2019) and synthetic carbonates in other labs (0.5255; Wostbrock et al., 2020a). The cause for this discrepancy is unknown but indicates that careful comparison of $\lambda_{calcite-water}$ across labs and different material types is needed. We explored the impact of $\lambda_{calcite-water}$ selection on our interpretations further in Section 6.2, but we note here that using higher $\lambda_{\text{calcite-water}}$ values $(\cong 0.5255)$ would yield $\Delta'^{17}O_{rfw}$ values ~26 per meg lower than waters in the Lake Junin region. which we consider unrealistic (Table S14; Figure S2). Raw data are provided in Table S7 to facilitate future recalculation using different $\lambda_{calcite-water}$ values.

342

343

344

345

346

347

325

326

327

328

329

330

331

332

333

334

335

336

337

338

339

340

341

6. Discussion:

6.1 Water isotopes

The isotopic composition of Junín precipitation is similar to that of precipitation elsewhere in the Peruvian Andes (Figure 3; e.g., Aron et al., 2021b; IAEA/WMO, 2022). In a $\delta^{18}\text{O-}\delta^2\text{H}$ plot, precipitation samples collected at Junín and Marcapomacocha (a GNIP station 45

km southwest of Junín) fall on or slightly above the GMWL, suggesting the importance of Rayleigh processes on the isotopic composition of regional precipitation (Dansgaard, 1964). The $\Delta'^{17}{\rm O}$ value of Junín amount-weighted annual precipitation, 31 ± 5 per meg, is within the range of semimonthly precipitation $\Delta'^{17}{\rm O}$ values in the Peruvian Altiplano (29–55 per meg; Figure 3; Aron et al., 2021b). Combining precipitation data from Junín and southern Peru, the regional meteoric water line: $\delta'^{17}{\rm O}{=}0.5277~(\pm0.0003)\times\delta'^{18}{\rm O}{+}0.0312~(\pm0.0031)$, lies between the global meteoric water line reported by Luz and Barkan (2010) and a recently updated compilation (Aron et al., 2021a; Table S11). Unfortunately, our precipitation dataset spans too short of a time interval to evaluate seasonal trends in $\Delta'^{17}{\rm O}$ values at Junín.

Surface water d-excess and $\Delta'^{17}O$ values are positively correlated in the Lake Junín region (Pearson's r= 0.94; Figure 3C), consistent with the influence of evaporation. The $\Delta'^{17}O$ -d-excess relationship is 1.3 ± 0.1 per meg/‰, which is similar to observations from a global compilation of surface waters (r= 0.73; 1.2 ± 0.1 per meg/‰; Aron et al., 2021a) and highly evaporated surface waters from the Chilean Altiplano (r= 0.94; 1.2 ± 0.1 per meg/‰; Voigt et al., 2021). In contrast, precipitation $\Delta'^{17}O$ -d-excess are weakly correlated, both in the Lake Junín region (r= 0.30) and elsewhere (e.g., Aron et al., 2021a). This weak correlation may reflect differences in how moisture source conditions affect oxygen and hydrogen isotopic fractionation (e.g., Aron et al., 2021b;2021a), but systematic, long-term studies of precipitation d-excess and $\Delta'^{17}O$ are needed to understand these relationships in the Andes.

6.2 Carbonate Isotopes

In the Lake Junín region, $T_{\Delta47}$ values of lake carbonates (7–17°C) overlap in range with surface water temperatures measured during our sampling in May 2019 (11–24°C) (Figures 5,S3;

Table 2). The measured water temperatures are more variable than carbonate $T_{\Delta 47}$ values and we consider them to represent snapshots of field work conditions (e.g., season, time of day) (Figure S3; Section 3.2.2). In contrast, carbonate samples integrate time (likely months—years). Average $T_{\Delta 47}$ for the Lake Junín region lakes is $13 \pm 3^{\circ}$ C, which is higher than MAT (6.5°C) and consistent with observations globally, where lake water temperatures are commonly elevated relative to mean air temperatures (Hren and Sheldon, 2012). This consideration is important when using lake carbonate $T_{\Delta 47}$ to infer paleo-temperatures, as it may be appropriate to consider lake carbonate $T_{\Delta 47}$ as a maximum estimate of MAT.

Bedrock carbonates yield high $T_{\Delta47}$ values (61 ±4°C) compared to the lacustrine carbonates (13 ±3°C) (Table 2, Figure 5B). The high bedrock carbonate temperatures are inconsistent with Earth surface conditions and likely reflect burial conditions (Huntington and Lechler, 2015). Bedrock temperatures of 60°C are consistent with burial of ~3 km based on ~20°C/km temperature gradients observed in boreholes in Peru (Henry and Pollack, 1988). We leverage these distinct temperature groupings to screen for detrital carbonate input into local lakes, as incorporation of detrital carbonate into lake sediments would result in unrealistically high lake carbonate $T_{\Delta47}$ values. Accordingly, low lacustrine $T_{\Delta47}$ values support the interpretation that lake carbonate isotope values record lake conditions, as opposed to a signal inherited from detrital material.

We then compare $\delta^{18}O$ values of reconstructed formation water from lacustrine carbonates ($\delta^{18}O_{rfw}$, derived from Δ_{47} measurements) to measured $\delta^{18}O$ values of lake water ($\delta^{18}O_{lake}$) collected at the same locations (Tables 2,S2). Paired $\delta^{18}O_{rfw}$ - $\delta^{18}O_{lake}$ values are positively correlated (r= 0.82, n= 8) and values fall close to a 1:1 line (Figure 5C), which suggests the isotopic composition of these carbonates reflects lake water at the time of carbonate

formation. The majority of $\delta^{18}O_{lake}$ and $\delta^{18}O_{rfw}$ values are higher than the $\delta^{18}O$ value of amount-weighted annual precipitation and track with lake hydrology, consistent with the influence of evaporation.

We also compare $\Delta'^{17}O$ of reconstructed formation water ($\Delta'^{17}O_{rfw}$) and measured lake waters ($\Delta'^{17}O_{lake}$) (Figure 5D). $\Delta'^{17}O_{rfw}$ values follow the same isotopic distribution as $\Delta'^{17}O_{lake}$ from the same catchments (Figure 4). However, $\Delta'^{17}O_{rfw}$ values are offset from paired $\Delta'^{17}O_{lake}$ values by -21 to 3 per meg (average: -11 per meg). We consider two possible explanations for this offset: 1) the selection of $\lambda_{calcite-water}$ is inappropriate for these carbonates, or 2) the carbonates and waters we collected are sampling different conditions.

Of these scenarios, we consider the first most likely. The value we use for $\lambda_{calcite-water}$ (0.5250; Section 5.2.3) was developed from laboratory-precipitated carbonate and may not represent the isotope effects that occur during lacustrine carbonate precipitation. A lower $\lambda_{calcite-water}$ value, e.g., 0.5246, would align $\Delta'^{17}O_{lake}$ and $\Delta'^{17}O_{rfw}$ values and is consistent with observed $\lambda_{calcite-water}$ values reported for some natural carbonates (Figure S2; Table S14) (Huth et al., 2022). Long-term calibration studies are needed to resolve $\lambda_{calcite-water}$ in lake systems. A second possibility is that sampled lake water $\Delta'^{17}O$ values do not represent lake water $\Delta'^{17}O$ at the time of carbonate formation. We sampled lakes in May, directly after the rainy season when local waters likely represent an evaporative minimum. This contrasts the dry season when carbonates likely formed and could explain why $\Delta'^{17}O_{lake}$ values are higher than $\Delta'^{17}O_{rfw}$ values. However, in this scenario, we would expect to see both a greater offset (more evaporation) in the larger lakes than the smaller lakes and a corresponding offset in $\delta^{18}O$, neither of which we observe (Figure 5C–D).

6.3 Reconstructing precipitation δ^{18} O

6.3.1 Modeling triple oxygen isotopes in lakes

Previous studies have used both isotope-enabled lake budget models and empirical data to establish the relationships between $\Delta'^{17}O$ values of precipitation, lake water, and paired mineral samples in highly evaporated, arid lake systems where lake water $\Delta'^{17}O$ and $\delta'^{18}O$ values are considerably distinct from input waters (Herwartz et al., 2017; Gázquez et al., 2018; Passey and Ji, 2019). In pursuit of developing triple oxygen isotopes to evaluate evaporative loss from lakes across a broad range of climates, we focus this study on data from modern lake systems in humid conditions with low evaporative loss (X_E) and model these conditions using steady-state lake budget equations.

6.3.2 Lake budget models

Using the same approach as Passey and Ji (2019), we apply Monte Carlo re-sampling to evaluate steady-state lake budget equations (Supplemental Script 2). In this mass balance approach, the isotopic composition of different reservoirs and volumetric fluxes and associated fractionations between reservoirs are used to calculate the isotopic composition of residual, evaporated lake waters (Figure S4; e.g., Benson and White, 1994; Passey and Ji, 2019).

In their modeling work, Passey and Ji (2019) restrict humidity to 0.3–0.7 to reflect their study area in the western U.S. (h= 0.42–0.55). For this work, we modeled lake water Δ'^{17} O under a range of humidity conditions to explore the humidity dependence of λ_{lake} (Figure 1). We expand the modeled humidity range to 0.3–0.9 to include the conditions of our study area where humidity is 0.7–0.9 (Tables S1,S15).

We use a lake budget equation that assumes i) lake waters are well mixed, ii) lake level is constant, iii) water is lost from the lake through a combination of evaporation, outflowing rivers, and/or groundwater, iv) waters entering the lake have a uniform isotopic composition and are relatively unevaporated, and v) evaporated moisture is integrated with atmospheric water vapor (Figure S4; Passey and Ji, 2019):

439

440

441

442

443

446

447

448

449

450

451

452

453

454

455

456

457

458

459

460

444
$$R_{W} = \frac{\alpha_{eq} R_{I} [\alpha_{diff} (1 - h) + h(1 - F)] + \alpha_{eq} h X_{E} R_{A} F}{X_{E} + \alpha_{eq} (1 - X_{E}) [\alpha_{diff} (1 - h) + h(1 - F)]}$$
445 (8)

We randomly sample values of X_E, h (relative humidity normalized to lake surface temperature), F (proportion of water vapor derived from upwind sources versus the lake itself), R_A (isotopic composition of atmospheric water vapor; calculated assuming equilibrium with precipitation), and α_{diff} , where $\alpha_{\text{diff}}=1.02849\Phi+(1-\Phi)$, (Φ is the relative proportion of diffusive transport (Φ = 1) versus turbulent transport (Φ = 0) of water vapor during evaporation and 1.02849 is the ¹⁸O/¹⁶O fractionation for pure molecular diffusion; Merlivat, 1978). Model conditions are listed in Table S15 and Supplemental Script 2. R_I (isotopic composition of input water) was defined as amount-weighted annual precipitation at Junín (Section 5.2.1) and lake temperature (used to calculate water vapor-liquid water equilibrium fractionation, α_{eq}) is 14°C. Each model simulation is conducted with 1000 random samplings of X_E , h, F, R_A , and Φ to produce unique combinations of modeled lake water ¹⁸O/¹⁶O and ¹⁷O/¹⁶O from which we calculate $\Delta'^{17}O$ and λ_{lake} values. We note that the choice of R_A has the greatest impact on the evaporation slope (λ_{lake}) at high humidity (as shown in plants by Landais et al., 2006); constraining R_A will be important for future refinement of model outputs in high humidity settings.

Before proceeding to discussion of the model output and the role of humidity on $\delta'^{18}O$ and $\Delta'^{17}O$ distributions in lakes, we want to explicitly note the limitation and utility of models. Mass balance models are representations of complex systems which can provide frameworks for evaluating and interpretating empirical observations. We recognize that models inherently simplify complex systems, such that not all model assumptions may always be met in natural environments. This does not preclude the utility of models, but users should exercise caution in selecting appropriate models and input parameters, particularly for ancient systems.

6.3.3 Model results and the role of humidity

We first compare model outputs to the observed $\delta'^{18}O$ and $\Delta'^{17}O$ values from the arid, western U.S. (Passey and Ji, 2019) and the humid, Lake Junín region (Figure 6A). The overlap in distributions of observed and modeled values for both regions makes sense; the isotopic values of unevaporated input waters of these regions are similar and the simulations consider a humidity range that reflects both areas. However, the unique $\Delta'^{17}O-\delta^{18}O$ and $\Delta'^{17}O-\lambda_{lake}$ relationships for each study are the result of regional humidity at the two sites. Specifically, humidity is tied to the proportion of kinetic fractionation during evaporation (in turn λ_{lake} is most sensitive to R_A at high humidity; Landais et al., 2006). This highlights a need to explore the influence of humidity on λ_{lake} further before we can effectively leverage λ_{lake} to quantify evaporation widely in different climatic systems.

When modeled humidity is restricted to reflect conditions for specific regions, the model output captures observations for that region. For example, the modeled isotopic composition for lakes in low humidity settings (0.3–0.7) are a good match with observations from the western U.S. (Figure 6B), but they fail to capture many of our observations from the Lake Junín region

where humidity is high. Correspondingly, the high humidity (0.7–0.9) solution space closely matches our observations in the Lake Junín region but not the observations from the arid western U.S. (Figure 6C).

To translate these relationships to ancient systems and use triple oxygen isotopes to reconstruct δ^{18} O values of unevaporated precipitation, we must also understand how humidity mediates the isotopic relationship between precipitation and lake water, or λ_{lake} , the evaporation slope in δ'^{18} O- δ'^{17} O space (Figure 1C-E) (Passey and Ji, 2019). Currently, our understanding of λ_{lake} relies primarily on highly evaporated systems in arid to hyper-arid environments (Table S12) (Herwartz et al., 2017; Surma et al., 2018; Passey and Ji, 2019; Voigt et al., 2021) and other climatic settings and hydrologic systems are under-represented (e.g., Pierchala et al., 2022). Passey and Ji (2019) showed that modeled λ_{lake} varies predictably as a function of Δ'^{17} O in low humidity (0.3–0.7) such that Δ'^{17} O_{lake} values can be used to model λ_{lake} for ancient systems. However, for this approach to be widely applicable, we must understand the dependence of triple oxygen evaporation slopes to humidity, which has been explored for plants (e.g., Landais et al., 2006) but not for lake systems, to our knowledge.

To address this gap, we evaluated the modeled relationship between λ_{lake} and $\Delta'^{17}O_{lake}$ with varying humidity. In Figure 6D-F we represent $\Delta'^{17}O$ as the difference between lake and input water $\Delta'^{17}O$ values ($\Delta'^{17}O_{lake}$ – $\Delta'^{17}O_{input}$) so we can consider data from study regions where input water $\Delta'^{17}O$ might vary. Figure 6D-F illustrates the distribution of modeled λ_{lake} values as a function of $\Delta'^{17}O$ for three different ranges of humidity. Our simulations affirm a strong relationship between λ_{lake} and $\Delta'^{17}O$ in all climate settings (Figure 6D) and show the potential to refine it where the humidity can be constrained (Figure 6E-F). The full humidity (0.3–0.9) model describes all observational data and can be reliably used to estimate λ_{lake} .

However, a simple sensitivity analysis shows that humidity plays an important role on modeled lake water $\Delta'^{17}O$ and λ_{lake} values when all other modeled variables are held constant (Figure S5). These results indicate λ_{lake} is most sensitive to humidity when $X_E \cong 0.3$, suggesting that using humidity to refine modeled values of λ_{lake} is most useful in flow-through lakes with a moderate amount of evaporation. Conversely under high evaporation scenarios ($X_E > 0.7$), the difference in modeled λ_{lake} at high and low humidity is minimized. Therefore, when X_E is low, constraining humidity is important for accurate estimates of λ_{lake} , but it is less important when X_E is high (>0.7). λ_{lake} has the largest effect on $\delta'^{18}O_{rucp}$ when the isotopic composition of lake water is very different from input water, as is commonly observed in arid, highly evaporated systems with very low $\Delta'^{17}O_{lake}$ (Figure S5C). Uncertainty in λ_{lake} has a smaller effect on reconstructed $\delta'^{18}O_{rucp}$ in humid, less evaporated systems.

We note that our modeled results produce some very low λ_{lake} values (<0.5185, endmember for diffusive vapor transport; Barkan and Luz, 2007) (Figure 6D-F). Generally, the very low modeled λ_{lake} values (~4% of solutions) are associated with very high relative humidity (h>0.8), low $\delta'^{18}O_{vapor}$ and $\Delta'^{17}O_{vapor}$ (-26 to -25‰ and 4 to 15 per meg, respectively) and primarily non-lake vapor sources (F>0.9); no clear relationship is observed between low λ_{lake} and Φ or X_E (Figure S6). While this combination of conditions could occur in nature, it would be rare. As a result, we expect most realistic λ_{lake} values to be 0.5185–0.529 (Barkan and Luz, 2007; Luz and Barkan, 2010).

We also observe that some carbonates from humid environments produced very low empirical λ_{lake} values (<0.5185). From the model results described above, we cannot rule out the role of climate on these low λ_{lake} values but we also recognize the substantial challenges in

determining a slope (λ_{lake}) between two points (i.e., input water and lake waters) that are very close together in their isotopic composition. In low X_E systems, $\delta^{18}O$ of input water and lake water are often close (<2‰), meaning that the error in selection or measurement of either will result in high uncertainty in the slope between the points (Figure S7). In high X_E systems, there is less uncertainty in determining λ_{lake} empirically as $\delta^{18}O$ values of input and lake water differ substantially. Accordingly, observations of λ_{lake} will always have high uncertainty when $\delta^{18}O$ of lake waters and precipitation are similar. This highlights the utility of using modeling approaches to evaluate λ_{lake} , particularly in humid settings (Figures 6D-F,S5,S7).

6.3.4 Improving reconstructed precipitation $\delta^{18}O$ estimates

Selection of modeled λ_{lake} is important when reconstructing precipitation $\delta^{18}O$ values $(\delta'^{18}O_{rucp})$ as λ_{lake} values that are too high will yield $\delta'^{18}O_{rucp}$ values that are lower than the true $\delta'^{18}O$ of input waters, while λ_{lake} slopes that are too low produce the opposite effect (Figure 1E). We conduct a sensitivity test to evaluate λ_{lake} under each of the three humidity scenarios presented in Section 6.3.3. We then use modeled λ_{lake} values to calculate $\delta'^{18}O_{rucp}$ ($\delta'^{18}O_{rucp} = \left[\Delta'^{17}O_{precip} - \Delta'^{17}O_{rfw} + (\lambda_{lake} - \lambda_{ref}) \times \delta'^{18}O_{ref}\right] / \left[\lambda_{lake} - \lambda_{ref}\right]$; Passey and Ji, 2019). Using the lake budget model, low humidity produces the highest modeled λ_{lake} values and lowest $\delta'^{18}O_{rucp}$ values, high humidity produces the lowest modeled λ_{lake} values and the highest $\delta'^{18}O_{rucp}$ values, and the full humidity model is in the middle (Figure 7; Table S16). λ_{lake} modeled at high humidity returns $\delta'^{18}O_{rucp}$ values (-15.2 $\pm 2.1\%$) that are most similar to amount-weighted annual precipitation (-14.1%) in the Lake Junín region (Figure 7). The full and low humidity models yield lower $\delta'^{18}O_{rucp}$ values (-16.2 $\pm 2.0\%$, -17.0 $\pm 2.0\%$, respectively). These

results highlight the value of considering local humidity (and other parameters in Eq. 8; e.g., R_A , F) when possible to improve accuracy of modeled λ_{lake} and $\delta'^{18}O_{rucp}$ values. The uncertainty in estimated $\delta'^{18}O_{rucp}$ values is a function of both uncertainty in λ_{lake} and $\Delta'^{17}O_{lake}$ (Passey and Ji, 2019), and should be evaluated on a case-to-case basis.

In each humidity scenario, estimated $\delta'^{18}O_{rucp}$ values are lower than $\delta'^{18}O$ values for amount-weighted mean precipitation. Possible explanations include a positive bias in modeled λ_{lake} , selection of $\lambda_{calcite-water}$ that is too high (Sections 5.2.3, 6.2), or estimated precipitation $\Delta'^{17}O$ or $\delta'^{18}O$ values that are too high, as also surmised by Passey and Ji (2019). Additional precipitation and lake water observations in different climate settings will continue to improve our understanding of all of the parameters above.

Notwithstanding continued refinement of λ_{lake} and $\Delta'^{17}O_{precip}$, we show how triple oxygen isotopes in carbonates and waters can be used alongside modeled λ_{lake} values to generate $\delta'^{18}O_{rucp}$ values close to amount-weighted annual precipitation (within ~1–2‰) in both arid and humid environments. In conjunction with other lines of evidence and proxy materials, $\Delta'^{17}O$ can help differentiate between lake systems with different hydrologic states (Figure 4), such that we can use $\Delta'^{17}O$ values to evaluate how hydrology influences lacustrine $\delta^{18}O$ records. This is essential for studies that use lakes to reconstruct past climate and hydrology, and for paleoelevation studies that rely on $\delta'^{18}O_{rucp}$ values (e.g., Ibarra et al., 2021; Kelson et al., 2022).

7. Conclusions

In this study, we present new isotope data ($\delta^{18}O$, $\delta^{17}O$, $\delta^{2}H$, Δ_{47} , $\Delta'^{17}O$, d-excess) from precipitation, surface waters, and lake carbonates in the Lake Junín region of Peru. We use these data alongside lake water isotope models run over a broad range of humidity conditions to

evaluate and improve the accuracy of precipitation δ^{18} O reconstructions derived from triple oxygen isotopes. From this work we conclude:

- 1. Formation water temperatures, derived from modern lake carbonate $T_{\Delta 47}$, are elevated compared to MAT, consistent with the growing dataset of Δ_{47} in lakes and analysis of lake temperatures globally.
- 2. In catchments containing carbonate bedrock influenced by high temperatures, $T_{\Delta 47}$ values of lake sediments can be used to screen for detrital inputs.
- 3. In the Lake Junín region, $\Delta'^{17}O$ values from four lakes reflect the X_E state of each lake, demonstrating that $\Delta'^{17}O$ measurements are effective for evaluating lake hydrology in both humid and arid lake systems.
- 4. $\delta^{18}O_{precip}$ values reconstructed using triple oxygen isotopic data from lakes are closest to observed mean-weighted $\delta^{18}O_{precip}$ values when humidity is known, but this approach provides accurate $\delta'^{18}O_{rucp}$ estimates even when humidity is unconstrained.

This work solidifies the interpretive framework for using $\Delta'^{17}O$ and Δ_{47} measurements in lake sediments to constrain temperature, lake hydrology, and $\delta^{18}O$ values of precipitation by extending it to humid systems and lakes with little evaporative water loss. Applicability of the $\Delta'^{17}O$ approach for constraining lake water evaporation across climate states and lake types, for either paleoclimate or paleoelevation studies, means that it can widely be applied to geologic archives where climate and/or hydrology may be unconstrained. While our study focuses on carbonate lakes, our results also apply to interpretations of $\Delta'^{17}O$ records from lakes with other mineral precipitates (e.g., silica, gypsum). Future work should focus on applying the $\Delta'^{17}O$ framework to constraining evaporation and $\delta'^{18}O_{rucp}$ values for ancient lake systems, including sediment records from Lake Junín.

597 **Data Availability:** All new water isotope data (δ^2 H, δ^{18} O, Δ'^{17} O) are available from the University of Utah Water 598 599 Isotope Database (https://wateriso.utah.edu/waterisotopes/). New carbonate isotope data (δ^{18} O, 600 δ^{13} C, Δ_{47}) are available from the EarthChem database (https://www.earthchem.org/data-access/). 601 Supplemental R Scripts (1–2) are available at 602 https://github.com/sarahakatz/Katz_etal_ModernLakeD17O_SupMat. 603 604 **Acknowledgements:** 605 The authors gratefully acknowledge the citizen scientists who aided our precipitation and surface 606 water collection efforts. We also thank Union College undergraduates Jordy Herbert, Tshering 607 Lama Sherpa, James Molloy, Mike Kaye, and Laura Piccirillo for assistance with sample 608 collection. Additionally, we thank Drew Gronewold for advice on Monte Carlo modeling; Tyler 609 Huth, Julia Kelson, Natalie Packard, and Nick Ellis for helpful discussions; and Drake Yarian, 610 Emily Beverly, Ryan Horwitz, Elise Pelletier, Jerry Li, and Anouk Verheyden for assistance with 611 analyses. We thank three anonymous reviewers for constructive feedback that improved the 612 quality of this work. 613 614 This work was supported financially by a Department of Earth and Environmental Sciences Scott 615 Turner Award, a GSA Graduate Student Research Award, and a GSA Kerry Kelts Research 616 Award to S.A.K.; University of Michigan Departmental Funding and U.S. National Science 617 Foundation funding (EAR-2102843) to N.E.L. and B.H.P.; Union College Funding and U.S. 618 National Science Foundation funding (EAR-1402076) to D.T.R. and D.P.G. The U.S. National

- 619 Science Foundation funded Union College's isotope ratio mass spectrometer and peripherals
- 620 (NSF-MRI #1229258).

References:

- Aron, P.G., Levin, N.E., Beverly, E.J., Huth, T.E., Passey, B.H., Pelletier, E.M., Poulsen, C.J.,
- Winkelstern, I.Z., and Yarian, D.A., 2021a, Triple oxygen isotopes in the water cycle:
- 624 Chemical Geology, v. 565, p. 1–23, doi:10.1016/j.chemgeo.2020.120026.
- Aron, P.G., Poulsen, C.J., Fiorella, R.P., Levin, N.E., Acosta, R.P., Yanites, B.J., and Cassel,
- 626 E.J., 2021b, Variability and Controls on δ^{18} O, d-excess, and Δ'^{17} O in Southern Peruvian
- Precipitation: Journal of Geophysical Research: Atmospheres, v. 126, p. 1–18,
- 628 doi:10.1029/2020JD034009.
- Barkan, E., and Luz, B., 2007, Diffusivity fractionations of H₂¹⁶O/H₂¹⁷O and H₂¹⁶O/H₂¹⁸O in air
- and their implications for isotope hydrology: Rapid Communications in Mass Spectrometry,
- v. 21, p. 2999–3005, doi:10.1002/rcm.3180.
- Barkan, E., and Luz, B., 2005, High precision measurements of ¹⁷O/¹⁶O and ¹⁸O/¹⁶O ratios in
- H₂O: Rapid Communications in Mass Spectrometry, v. 19, p. 3737–3742,
- 634 doi:10.1002/rcm.2250.
- Benson, L. V, and White, J.W., 1994, Stable Isotopes of Oxygen and Hydrogen in the Truckee
- River Pyramid Lake Surface-Water System .1. Data-Analysis and Extraction of
- Paleoclimatic Information: Limnology and Oceanography, v. 39, p. 344–355.
- Bird, B.W., Abbott, M.B., Rodbell, D.T., and Vuille, M., 2011a, Holocene tropical South
- American hydroclimate revealed from a decadally resolved lake sediment δ^{18} O record:
- Earth and Planetary Science Letters, v. 310, p. 192–202, doi:10.1016/J.EPSL.2011.08.040.
- Bird, B.W., Abbott, M.B., Vuille, M., Rodbell, D.T., Stansell, N.D., and Rosenmeier, M.F.,
- 2011b, A 2,300-year-long annually resolved record of the South American summer
- monsoon from the Peruvian Andes: Proceedings of the National Academy of Sciences, v.

- 644 108, p. 8583–8588, doi:10.1073/pnas.1003719108.
- Bonifacie, M., Calmels, D., Eiler, J.M., Horita, J., Chaduteau, C., Vasconcelos, C., Katz, A.,
- Passey, B.H., and Ferry, J.M., 2017, Experimental calibration of the dolomite clumped
- isotope thermometer from 25 to 350°C, and implications for the temperature estimates for
- all (Ca, Mg, Fe) CO₃ carbonates digested at high temperature: Geochimica et
- 649 Cosmochimica Acta, v. 200, p. 255–279, doi:10.1016/j.gca.2016.11.028.
- 650 Cobbing, J., Quispesivana, L.Q., and Paz, M.M., 1996, Geologia de los cuadrangulos de Ambo,
- 651 Cerro de Pasco y Ondores. Boletin N77 Serie A: Carta Geológica Nacinonal.
- Dansgaard, W., 1964, Stable isotopes in precipitation: Tellus, v. 16, p. 436–468,
- doi:10.3402/tellusa.v16i4.8993.
- Dennis, K.J., Affek, H.P., Passey, B.H., Schrag, D.P., and Eiler, J.M., 2011, Defining an absolute
- reference frame for "clumped" isotope studies of CO₂: Geochimica et Cosmochimica Acta,
- 656 v. 75, p. 7117–7131, doi:10.1016/j.gca.2011.09.025.
- 657 Eiler, J.M., 2007, "Clumped-isotope" geochemistry-The study of naturally-occurring, multiply-
- substituted isotopologues: Earth and Planetary Science Letters, v. 262, p. 309–327,
- doi:10.1016/j.epsl.2007.08.020.
- Eiler, J.M., 2011, Paleoclimate reconstruction using carbonate clumped isotope thermometry:
- Quaternary Science Reviews, v. 30, p. 3575–3588, doi:10.1016/j.quascirev.2011.09.001.
- Flusche, M.A., Seltzer, G., Rodbell, D., Siegel, D., and Samson, S., 2005, Constraining water
- sources and hydrologic processes from the isotopic analysis of water and dissolved
- strontium, Lake Junin, Peru: Journal of Hydrology, v. 312, p. 1–13,
- doi:10.1016/j.jhydrol.2005.02.021.
- 666 Gázquez, F., Morellón, M., Bauska, T., Herwartz, D., Surma, J., Moreno, A., Staubwasser, M.,

- Valero-Garcés, B., Delgado-Huertas, A., and Hodell, D.A., 2018, Triple oxygen and
- hydrogen isotopes of gypsum hydration water for quantitative paleo-humidity
- reconstruction: Earth and Planetary Science Letters, v. 481, p. 177–188,
- doi:10.1016/j.epsl.2017.10.020.
- 671 Guo, W., and Zhou, C., 2019, Triple oxygen isotope fractionation in the DIC-H₂O-CO₂ system:
- A numerical framework and its implications: Geochimica et Cosmochimica Acta, v. 246, p.
- 673 541–564, doi:10.1016/j.gca.2018.11.018.
- Henry, S.G., and Pollack, H.N., 1988, Terrestrial heat flow above the Andean subduction zone in
- Bolivia and Peru: Journal of Geophysical Research, v. 93, p. 153–162,
- doi:10.1029/jb093ib12p15153.
- Herwartz, D., Surma, J., Voigt, C., Assonov, S., and Staubwasser, M., 2017, Triple oxygen
- isotope systematics of structurally bonded water in gypsum: Geochimica et Cosmochimica
- 679 Acta, v. 209, p. 254–266, doi:10.1016/j.gca.2017.04.026.
- Horton, T.W., Defliese, W.F., Tripati, A.K., and Oze, C., 2016, Evaporation induced ¹⁸O and ¹³C
- enrichment in lake systems: A global perspective on hydrologic balance effects: Quaternary
- Science Reviews, v. 131, p. 365–379, doi:10.1016/j.quascirev.2015.06.030.
- Hren, M.T., and Sheldon, N.D., 2012, Temporal variations in lake water temperature:
- Paleoenvironmental implications of lake carbonate δ^{18} O and temperature records: Earth and
- Planetary Science Letters, v. 337–338, p. 77–84, doi:10.1016/j.epsl.2012.05.019.
- Hulston, J.R., and Thode, H.G., 1965, Variations in the S³³, S³⁴, and S³⁶ contents of meteorites
- and their relation to chemical and nuclear effects: Journal of Geophysical Research, v. 70, p.
- 688 3475–3484, doi:10.1029/JZ070i014p03475.
- Huntington, K.W., and Lechler, A.R., 2015, Carbonate clumped isotope thermometry in

- continental tectonics: Tectonophysics, v. 647–648, p. 1–20,
- doi:10.1016/j.tecto.2015.02.019.
- Huntington, K.W., Saylor, J., Quade, J., and Hudson, A.M., 2015, High late Miocene-Pliocene
- 693 elevation of the Zhada Basin, southwestern Tibetan Plateau, from carbonate clumped
- isotope thermometry: Bulletin of the Geological Society of America, v. 127, p. 181–199,
- 695 doi:10.1130/B31000.1.
- Huntington, K.W., Wernicke, B.P., and Eiler, J.M., 2010, Influence of climate change and uplift
- on Colorado Plateau paleotemperatures from carbonate clumped isotope thermometry:
- 698 Tectonics, v. 29, p. 1–19, doi:10.1029/2009TC002449.
- Huth, T.E., Passey, B.H., Cole, J.E., Lachniet, M.S., McGee, D., Denniston, R.F., Truebe, S., and
- Levin, N.E., 2022, A framework for triple oxygen isotopes in speleothem paleoclimatology:
- 701 Geochimica et Cosmochimica Acta, v. 319, p. 191–219, doi:10.1016/j.gca.2021.11.002.
- 702 IAEA/WMO, 2022, Global Network of Isotopes in Precipitation (GNIP):,
- 703 https://www.iaea.org/services/networks/gnip.
- Total Tibarra, D.E., Kukla, T., Methner, K.A., Mulch, A., and Chamberlain, C.P., 2021, Reconstructing
- Past Elevations From Triple Oxygen Isotopes of Lacustrine Chert: Application to the
- Eocene Nevadaplano, Elko Basin, Nevada, United States: Frontiers in Earth Science, v. 9, p.
- 707 1–19, doi:10.3389/feart.2021.628868.
- Kelson, J.R., Petersen, S. V., Niemi, N.A., Passey, B.H., and Curley, A.N., 2022, Looking
- upstream with clumped and triple oxygen isotopes of estuarine oyster shells in the early
- Eocene of California, USA: Geology, doi:10.1130/G49634.1.
- Kim, S.-T., and O'Neil, J.R., 1997, Equilibrium and nonequilibrium oxygen isotope effects in
- synthetic carbonates: Geochimica et Cosmochimica Acta, v. 61, p. 3461–3475,

- 713 doi:10.1016/S0016-7037(97)00169-5.
- Landais, A., Barkan, E., Yakir, D., and Luz, B., 2006, The triple isotopic composition of oxygen
- 715 in leaf water: Geochimica et Cosmochimica Acta, v. 70, p. 4105–4115,
- 716 doi:10.1016/j.gca.2006.06.1545.
- Leng, M.J., and Marshall, J.D., 2004, Palaeoclimate interpretation of stable isotope data from
- 718 lake sediment archives: Quaternary Science Reviews, v. 23, p. 811–831,
- 719 doi:10.1016/J.QUASCIREV.2003.06.012.
- Luz, B., and Barkan, E., 2010, Variations of ¹⁷O/¹⁶O and ¹⁸O/¹⁶O in meteoric waters: Geochimica
- 721 et Cosmochimica Acta, v. 74, p. 6276–6286, doi:10.1016/j.gca.2010.08.016.
- Merlivat, L., 1978, Molecular diffusitivies or H₂¹⁶O, HD¹⁶O, and H₂¹⁸O in gases: The Journal of
- 723 Chemical Physics, v. 69, doi:10.1063/1.436884.
- Miller, M.F., and Pack, A., 2021, Why Measure ¹⁷O? Historical Perspective, Triple-Isotope
- Systematics and Selected Applications: Reviews in Mineralogy and Geochemistry, v. 86, p.
- 726 1–34, doi:10.2138/rmg.2021.86.01.
- Passey, B.H., Hu, H., Ji, H., Montanari, S., Li, S., Henkes, G.A., and Levin, N.E., 2014, Triple
- oxygen isotopes in biogenic and sedimentary carbonates: Geochimica et Cosmochimica
- 729 Acta, v. 141, p. 1–25, doi:10.1016/j.gca.2014.06.006.
- Passey, B.H., and Ji, H., 2019, On the use of triple oxygen isotopes in lake waters and carbonates
- for reconstructing δ^{18} O of unevaporated precipitation: a case study from the Western United
- 732 States: Earth and Planetary Science Letters, v. 518, p. 1–12, doi:10.1016/j.epsl.2019.04.026.
- Passey, B.H., Levin, N.E., Cerling, T.E., Brown, F.H., and Eiler, J.M., 2010, High-temperature
- environments of human evolution in East Africa based on bond ordering in paleosol
- carbonates: Proceedings of the National Academy of Sciences, v. 107, p. 11245–11249,

- 736 doi:10.1073/pnas.1001824107.
- Petersen, S.V. V. et al., 2019, Effects of Improved ¹⁷O Correction on Inter-Laboratory
- Agreement in Clumped Isotope Calibrations, Estimates of Mineral-Specific Offsets, and
- 739 Temperature Dependence of Acid Digestion Fractionation: Geochemistry, Geophysics,
- 740 Geosystems, v. 20, p. 3495–3519, doi:10.1029/2018GC008127.
- Petryshyn, V.A., Lim, D., Laval, B.L., Brady, A., Slater, G., and Tripati, A.K., 2015,
- Reconstruction of limnology and microbialite formation conditions from carbonate clumped
- 743 isotope thermometry: Geobiology, v. 13, p. 53–67, doi:10.1111/gbi.12121.
- Pierchala, A., Rozanski, K., Dulinski, M., and Gorczyca, Z., 2022, Triple-isotope mass balance
- of mid-latitude, groundwater controlled lake: Science of The Total Environment, v. 814, p.
- 746 1–11, doi:10.1016/j.scitotenv.2021.151935.
- Schauble, E.A., Ghosh, P., and Eiler, J.M., 2006, Preferential formation of ¹³C–¹⁸O bonds in
- carbonate minerals, estimated using first-principles lattice dynamics: Geochimica et
- 749 Cosmochimica Acta, v. 70, p. 2510–2529, doi:10.1016/j.gca.2006.02.011.
- 750 Schoenemann, S.W., Schauer, A.J., and Steig, E.J., 2013, Measurement of SLAP2 and GISP
- δ^{17} O and proposed VSMOW-SLAP normalization for δ^{17} O and δ^{1
- Communications in Mass Spectrometry, v. 27, p. 582–590, doi:10.1002/rcm.6486.
- 753 Seltzer, G., Rodbell, D., and Burns, S., 2000, Isotopic evidence for late Quaternary climatic
- change in tropical South America: Geology, v. 28, p. 35–38.
- 755 SENAMHI, 2022, Datos Hidrometeorológicos a nivel nacional:,
- https://www.senamhi.gob.pe/?&p=estaciones (accessed November 2019).
- Surma, J., Assonov, S., Herwartz, D., Voigt, C., and Staubwasser, M., 2018, The evolution of
- 758 ¹⁷O-excess in surface water of the arid environment during recharge and evaporation:

759	Scientific Reports, v. 8, p. 4972, doi:10.1038/s41598-018-23151-6.
760	Voigt, C., Herwartz, D., Dorador, C., and Staubwasser, M., 2021, Triple oxygen isotope
761	systematics of evaporation and mixing processes in a dynamic desert lake system:
762	Hydrology and Earth System Sciences, v. 25, p. 1211-1228, doi:10.5194/hess-25-1211-
763	2021.
764	Wang, Z., Schauble, E.A., and Eiler, J.M., 2004, Equilibrium thermodynamics of multiply
765	substituted isotopologues of molecular gases: Geochimica et Cosmochimica Acta, v. 68, p.
766	4779–4797, doi:10.1016/j.gca.2004.05.039.
767	Wostbrock, J.A.G., Brand, U., Coplen, T.B., Swart, P.K., Carlson, S.J., Brearley, A.J., and
768	Sharp, Z.D., 2020a, Calibration of carbonate-water triple oxygen isotope fractionation:
769	Seeing through diagenesis in ancient carbonates: Geochimica et Cosmochimica Acta, v.
770	288, p. 369–388, doi:10.1016/j.gca.2020.07.045.
771	Wostbrock, J.A.G., Cano, E.J., and Sharp, Z.D., 2020b, An internally consistent triple oxygen
772	isotope calibration of standards for silicates, carbonates and air relative to VSMOW2 and
773	SLAP2: Chemical Geology, p. 1–9, doi:10.1016/j.chemgeo.2019.119432.
774	Young, E.D., Galy, A., and Nagahara, H., 2002, Kinetic and equilibrium mass-dependent isotope
775	fractionation laws in nature and their geochemical and cosmochemical significance:
776	Geochimica et Cosmochimica Acta, v. 66, p. 1095–1104.
777	

Figures:

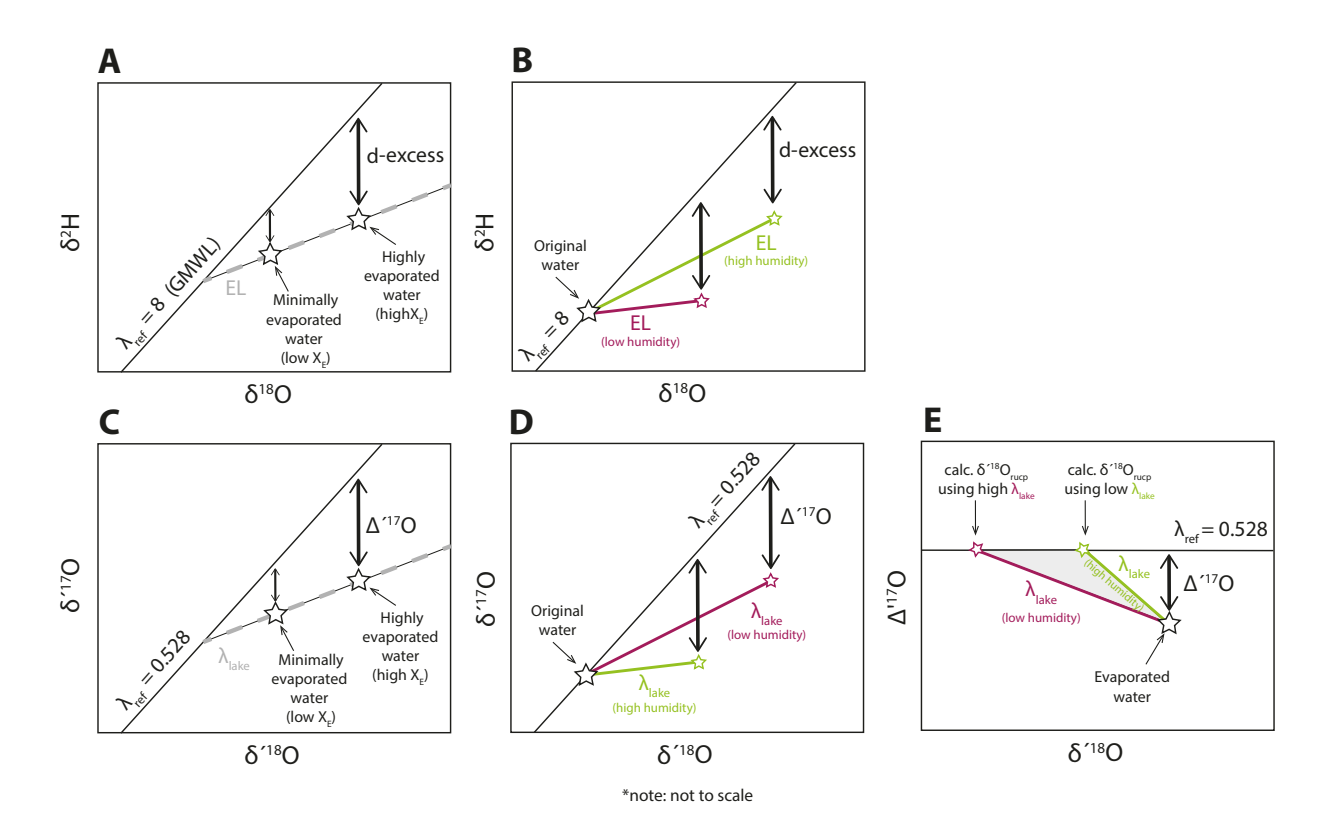


Figure 1. Schematics for oxygen and hydrogen isotope fractionation in waters. For $\delta^{18}\text{O}-\delta^2\text{H}$ distributions, (A) shows how evaporated waters fall along a shallower Evaporation Line (EL) slope than the Global Meteoric Water Line (GMWL) and (B) shows how the isotopic composition of evaporated waters is related to unevaporated input water; colored lines represent EL slopes under varying humidity conditions. For $\delta'^{18}\text{O}-\delta'^{17}\text{O}$ space, in (C) $\Delta'^{17}\text{O}$ quantifies deviations from a reference slope (λ_{ref}) along a shallower evaporation slope, λ_{lake} , and (D) shows variation in evaporation slope, λ_{lake} , under varying humidity conditions. The schematic in (E) highlights the influence of λ_{lake} (and by extension, humidity) on the calculated $\delta'^{18}\text{O}$ value of unevaporated precipitation ($\delta'^{18}\text{O}_{rucp}$). The two humidity scenarios shown in panels B, D, and E, highlight the relationships between humidity, λ_{lake} , and d-excess (B) or $\Delta'^{17}\text{O}$ (D-E). Note: not to

790 scale.

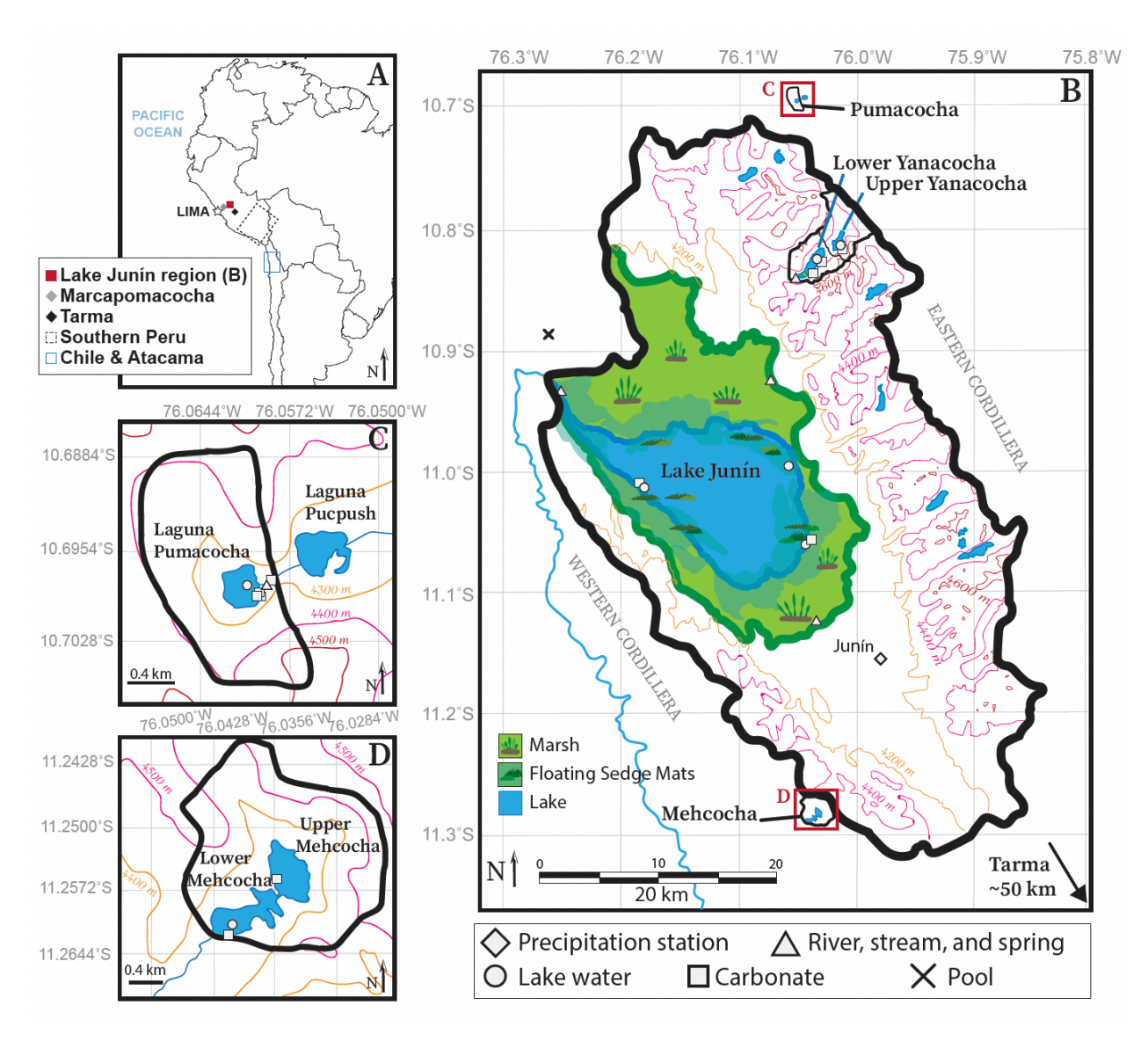


Figure 2. Maps of the study region. (A) Map of South America with the Lake Junín region indicated by a red box. (B) Topographic map of the Lake Junín and Yanacocha watersheds, with 200 m elevation contours. Note that the Yanacocha watershed is a glacially carved catchment located within the larger Lake Junín catchment. Red boxes indicate the locations of panels C and D. (C) Topographic map of the Pumacocha watershed (elevation contours 100 m). (D) Topographic map of the Mehcocha watershed (elevation contours 100 m). In B-D, watershed

boundaries are indicated by solid black lines. The approximate locations of samples selected for $\Delta'^{17}O$ analysis are indicated for each watershed (see legend below panel B); for clarity, we do not plot the locations of all surface water samples analyzed in this study (n = 140). Coordinates for precipitation stations, water samples, and carbonates are provided in Tables S1–S2, and 2.

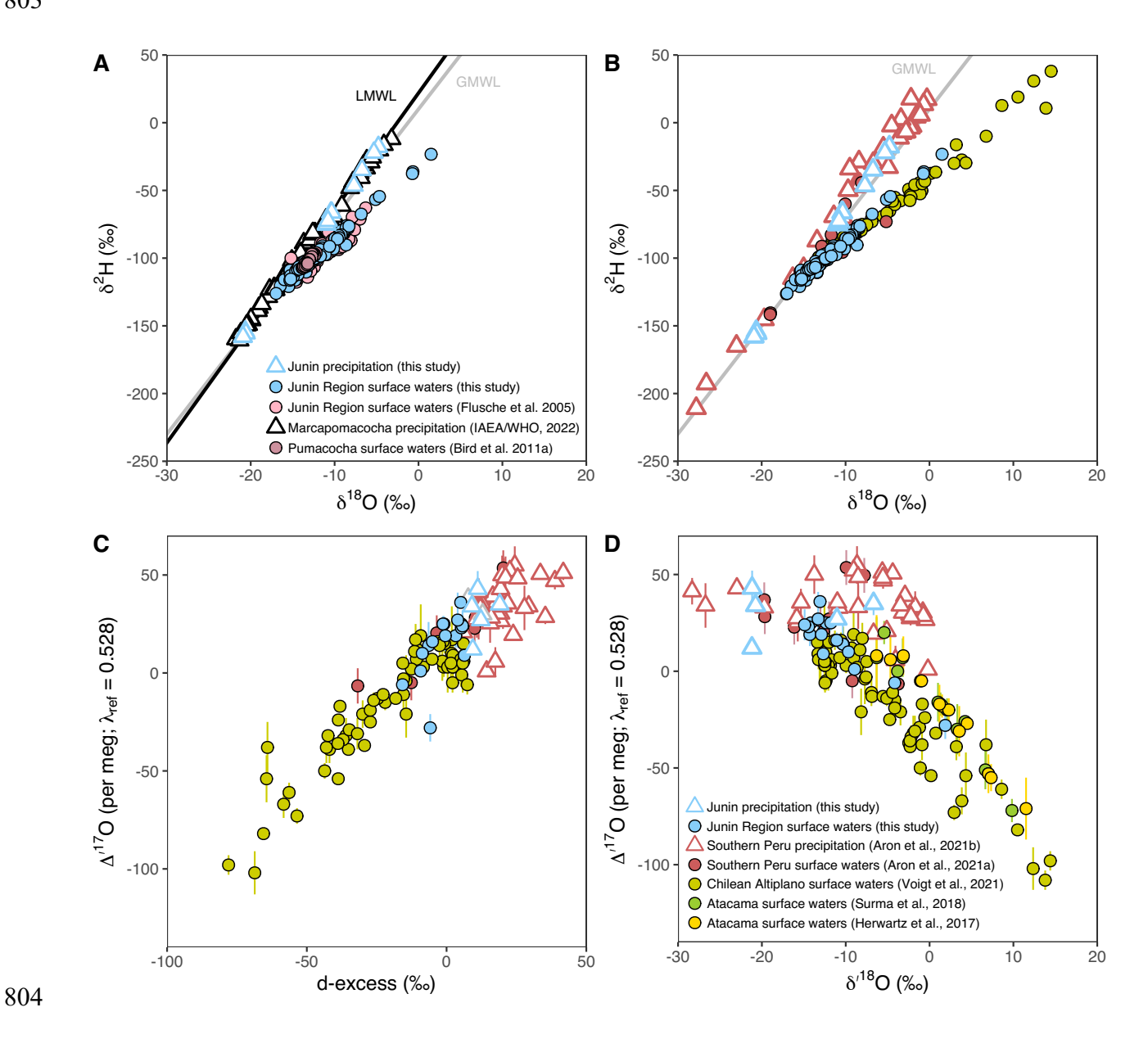


Figure 3. (A-B) Plot of precipitation and surface water $\delta^{18}O$ and $\delta^{2}H$ values from the (A) Lake Junín region and (B) central Andes. The Global Meteoric Water Line (GMWL), $\delta^{2}H = 8*\delta^{18}O +$

10, is shown as a grey line for reference. In (A), the Local Meteoric Water Line (LMWL) for Junín precipitation ($\delta^2 H = 8.6*\delta^{18}O + 21.9$) is shown as a black line. (C-D) Published water data from central Andean studies that report triple oxygen isotope values; the legend shown in panel D represents data plotted in panels B-D. (C) Plot of $\Delta'^{17}O$ and d-excess values. Error bars represent the 1 σ uncertainty reported in each study. (D) Plot of $\Delta'^{17}O$ versus $\delta'^{18}O$. Note that Herwartz et al. (2017) and Surma et al. (2018) did not report hydrogen isotope data, so data from those studies are only plotted in panel D.



807

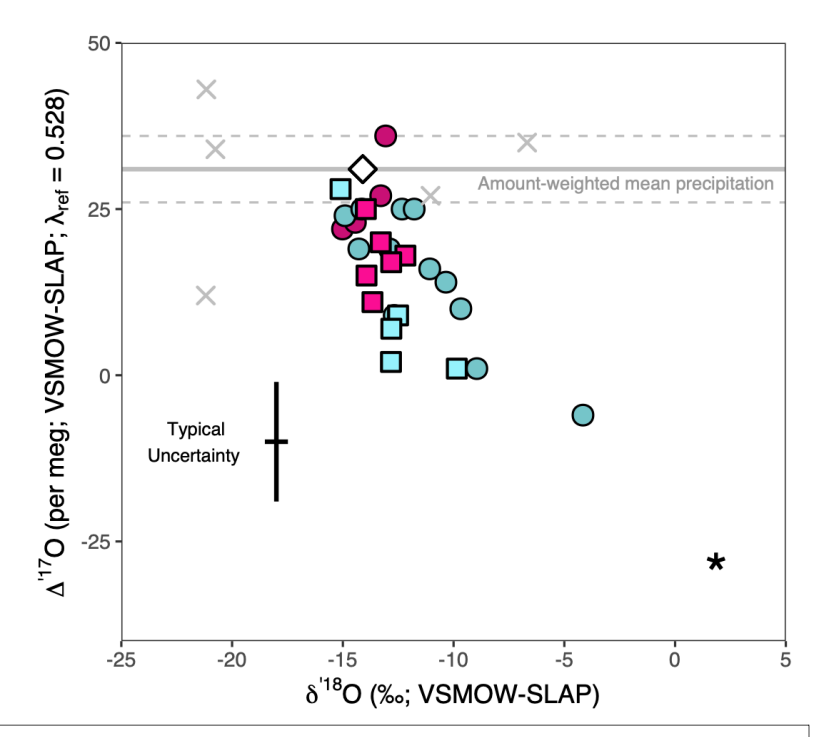
808

809

810

811

812



- ♦ Amount weighted mean annual precipitation
- × Monthly precipitation
- Water from small watersheds, little evaporation
- Reconstructed formation water from small watersheds, little evaporation
- Water from large watersheds, more evaporation
- Reconstructed formation water from large watersheds, more evaporation
- * Isolated pool (pan evaporation)

Figure 4. Triple oxygen isotope data of surface waters and carbonate formation waters from the Lake Junín region. Mehcocha and Pumacocha are categorized as small watersheds and Yanacocha and Lake Junín are categorized as large watersheds (see Section 3.1). Solid and dashed horizontal grey lines represent amount-weighted annual precipitation $\Delta'^{17}O$ and the 1 σ uncertainty, respectively (31 ±5 per meg). The "Typical Uncertainty" is shown as the 1 σ standard deviation for $\Delta'^{17}O$ (=9 per meg) and $\delta'^{18}O$ (=0.5‰) based on the pooled standard deviation of water standards (Table S9).



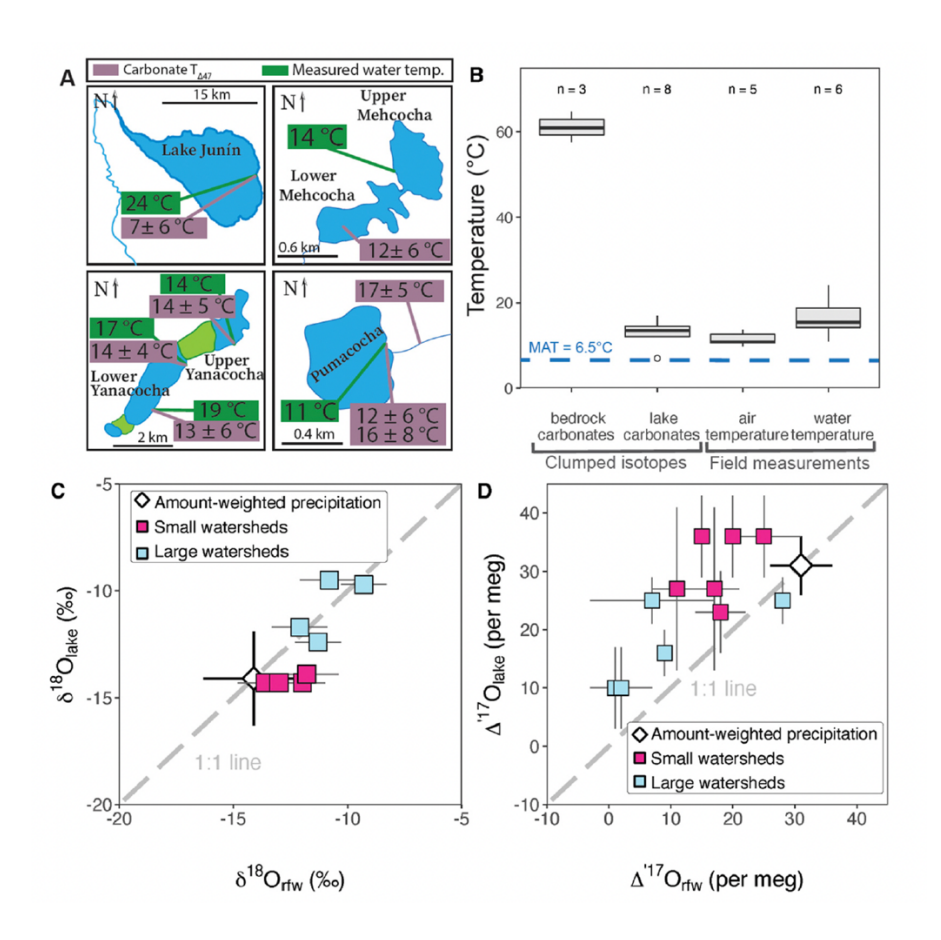


Figure 5. (A) Simplified maps of the four lakes illustrating carbonate $T_{\Delta 47}$ and surface water temperatures measured at time of sample collection. (B) Box and whisker plots show temperatures for bedrock and lake carbonate derived from clumped isotopes, and measurements

of air and water temperatures taken at the time of sample collection in May 2019. The central line of the box illustrates population medians; upper and lower hinges mark quantile boundaries; outliers are represented by open circles. A dashed horizontal line indicates mean annual temperature (MAT= 6.5°C) for reference. (C) δ^{18} O values of reconstructed carbonate formation waters (δ^{18} O_{rfw}) versus lake waters (δ^{18} O_{lake}) collected at the same locations. (D) Δ'^{17} O values of reconstructed carbonate formation waters (Δ'^{17} O_{rfw}) versus lake water Δ'^{17} O (Δ'^{17} O_{lake}) values from waters collected at the same sampling locations. In C-D, symbols are color coded based on categorization of catchment size (e.g., small = pink; large = blue). Error bars on δ^{18} O_{rfw}, Δ'^{17} O_{lake}, and Δ'^{17} O_{rfw} represent 1 σ standard deviations of replicate analyses. In panel C, uncertainty on δ^{18} O_{lake} is long term instrument precision (0.3 ‰) and is smaller than the size of the symbols. In panel D, long term analytical precision of 9 per meg for waters is used when replicate analyses of Δ'^{17} O_{lake} are unavailable. Data from these plots can be found in Tables 2–3, S2.

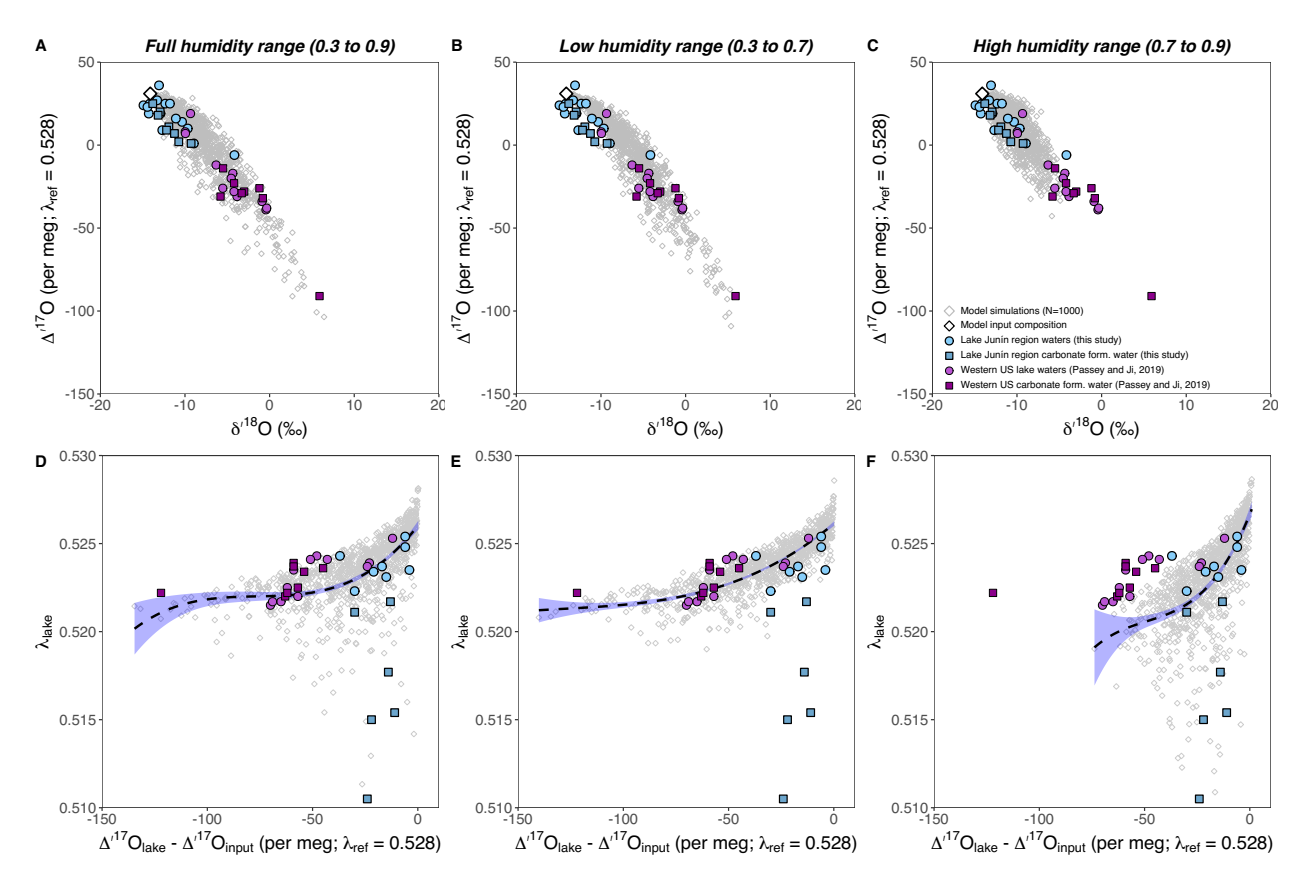


Figure 6. Comparison of observed and modeled triple oxygen isotope compositions for modern lakes (see Section 6.3.2; Eq. 8; Supplemental Script 2). Panels A-C illustrate 1000 model solutions (grey diamonds) for lake water $\Delta'^{17}O$ and $\delta'^{18}O$ derived from unevaporated input water $(\Delta'^{17}O=31 \text{ per meg}; \delta'^{18}O=-14.1\%$; represented by a white diamond). Each column represents different inputs for humidity across an X_E (evaporative loss / inputs) range of 0.01 to 1.0 (see Table S15 for run parameters). Panels D-F plot modeled $\Delta'^{17}O$ (shown as $\Delta'^{17}O_{lake}-\Delta'^{17}O_{input}$) versus modeled λ_{lake} (grey diamonds). A dashed black line shows a third-order polynomial fit for each model dataset and the shaded envelope represents the 95% CI. Note that in Panels D-F the y-axis scale is cropped to 0.510-0.530 to show realistic solutions which fall between equilibrium ($\lambda_{eq}=0.529$; Barkan and Luz, 2005) and diffusive ($\lambda_{diff}=0.5185$; Barkan and Luz, 2007) values. Empirically calculated values of λ_{lake} from lake waters, outflow rivers, and carbonate

datapoints than Panels A-C. The starting water in our model runs reflects local precipitation and is slightly different than starting water used by Passey and Ji ($\Delta'^{17}O=32$ per meg and $\delta'^{18}O=-15\%$), however, this does not affect the overall trends in the modeled isotopic	reconstructed formation waters are superimposed on modeled data (Table S12). Note that
is slightly different than starting water used by Passey and Ji (Δ'^{17} O= 32 per meg and δ'^{18} O= -15‰), however, this does not affect the overall trends in the modeled isotopic	samples outside the cropped frame are excluded, such that Panels D-F have fewer sample
$\delta'^{18}O=-15\%$), however, this does not affect the overall trends in the modeled isotopic	datapoints than Panels A-C. The starting water in our model runs reflects local precipitation and
	is slightly different than starting water used by Passey and Ji ($\Delta'^{17}O=32$ per meg and
distribution for lake water.	$\delta'^{18}O=-15\%$), however, this does not affect the overall trends in the modeled isotopic
	distribution for lake water.

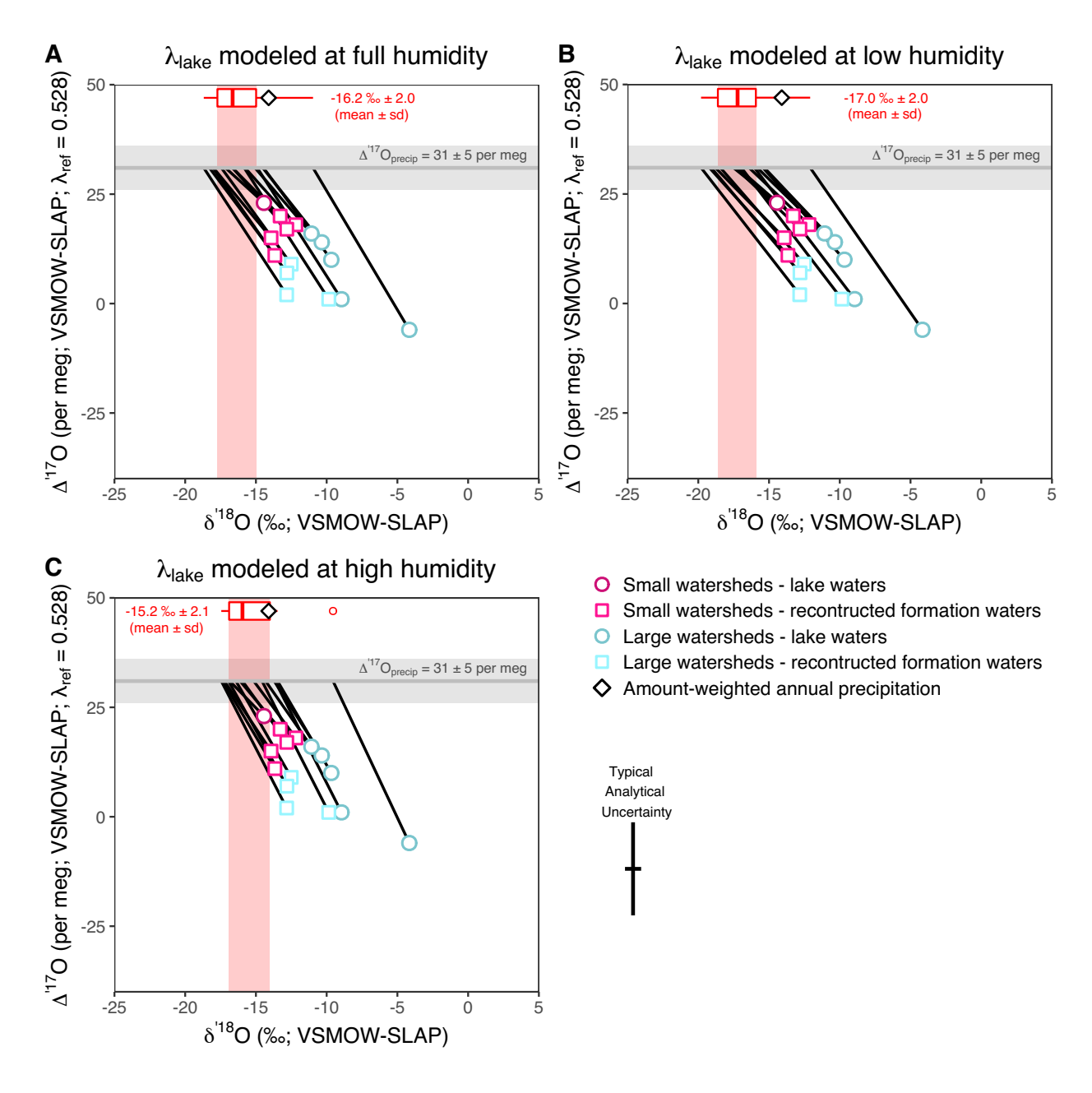


Figure 7. Plots of Δ'^{17} O versus δ'^{18} O showing the samples used in back projection trajectories (black lines, equivalent to λ_{lake}) for different ranges in humidity: A) full humidity 0.3–0.9, B) low humidity 0.3–0.7, C) high humidity 0.7–0.9. δ'^{18} O_{rucp} values for each humidity range are represented by the red box and whisker plots. The central line of the box illustrates sample medians; upper and lower hinges illustrate quantile boundaries; outliers are represented by open circles. A vertical red box demarks the interquartile range in δ'^{18} O_{rucp} values. Δ'^{17} O_{rfw} values

were calculated using $\lambda_{calcite-water} = 0.5250$. Note that we did not calculate $\delta'^{18}O_{rucp}$ values for samples with $\Delta'^{17}O$ values that are indistinguishable from precipitation (31 ± 5 per meg, represented by a horizontal grey box).

871

872

873

868

869

870

Tables:

Table 1. Summary and descriptions of the locations referred to in this text

Name	Description
Lake Junin region	The geographic area in which samples were collected (approx. 10.6-11.3°S and 75.8-76.3 °W)
Junín region	Department of Junín (Peruvian geopolitical region; approx. 10.7-12.6°S and 73.4-76.5 °W)
Junín	Town of Junín, Peru (11.15 °S; 75.00 °W)
Marcapomacocha	Town of Marcapomacocha and site of IAEA GNIP station (11.40 °S; 76.33 °W)
Pumacocha	Laguna Pumacocha watershed (10.70 °S; 76.06 °W)
Mehcocha ¹	Laguna Mehcocha watershed (11.26 °S; 76.04 °W)
Yanacocha	Laguna Yanacocha watershed (10.84 °S; 76.04 °W)
Lake Junin ²	Lake Junín watershed (11.00 °S; 76.10 °W)

¹ The offical name for this lake is Laguana Catucana, note that "Mehcocha" is an informal name.

874

875

Table 2. Summary of carbonate samples and isotope data from the Lake Junin region

² Lake Junin is also known as *Chinchaycocha* or *Chinchayqucha* in Quechua.

THOR TO DOWN	Table 2: Summary of mare call bounds samples and Botope care from the Lane Summit	samples and isotope da	ta mom the rank outlin													
	Sample Name	Depositional environment	Material Type	Latitude (°S)	Longitude (°W)	Air Temperature ^A (°C)	Water Temperature ^A (°C)	Number of replicate Δ_{47} analyses	Number of replicate Δ ¹⁷ O analyses		δ ¹³ C _{GCO3} B δ ¹⁸ O _{GCO3} B(%, W, PDB) VSMOW)	Δ_{t7}^{D} (%) $\Gamma_{\Delta t7}^{E}$ (°C)	Tan E (°C)	δ ¹⁸ O _{rfw} ^F (‰, VSMOW)	A' ¹⁷ O _{CaCO3} (per meg; VSMOW- SLAP)	A ¹⁷ O _{rfw} ^G (per meg; VSMOW- SLAP)
	PE19-PUM-C007	shallow, nearshore	micrite sediment	10.6977	76.0599	1	11	3	2	$-2.67 (\pm 0.08)$	$17.15 (\pm 0.10)$	$0.644 (\pm 0.013)$	12 (± 6)	$-13.6 (\pm 1.2)$	(9 +) 29-	25
-	PE19-PUM-C008	shallow, nearshore	micrite sediment	10.6977	76.0599	1	11	2	-	$-2.64 (\pm 0.01)$	$17.15 (\pm 0.02)$	$0.633 (\pm 0.021)$	16 (±8)	$-13.0 (\pm 1.6)$	-70	20
Pulliacocha	PE19-PUM-C021	shallow, nearshore	micrite sediment	10.6977	76.0599	1	11	1	2	1	17.02 (± 0.15) ^C		,		$-77 (\pm 0)$	15
	PE19-PUM-C133	outflow stream	rinds on cobbles	10.6976	76.0589	1	11	2	2	$-3.74 (\pm 0.02)$	$17.80 (\pm 0.13)$	$0.628 (\pm 0.002)$	17 (± 5)	$-12.0 (\pm 1.0)$	-71 (± 4)	18
Mehoooha	PE19-MEH-C117	deep, open water	micrite sediment	11.2618	76.0401			3	2	$0.14 (\pm 0.09)$	19.09 (± 0.13)	$0.644 (\pm 0.017)$	12 (± 6)	-11.8 (± 1.4)	-81 (± 4)	11
Melicociia	PE19-MEH-C122	shallow, nearshore	micrite sediment	11.2574	76.0352	8.6	14.3	1	2	1	18.16 (± 0.61) ^C			1	-76 (± 4)	17
	PE19-YAN-C156	shallow, nearshore	micrite sediment	10.8495	76.0449	10.8	16.6	2	2	$-0.51 (\pm 0.01)$	21.32 (± 0.20)	0.639 (± 0.002)	14 (± 4)	-9.3 (± 1.0)	-90 (± 4)	1
Yanacocha	PE19-YAN-C158	shallow, nearshore	micrite sediment	10.8532	76.0506	10.6	19.4	3	2	$-1.09 (\pm 0.05)$	$20.05 (\pm 0.10)$	$0.643 (\pm 0.016)$	13 (± 6)	$-10.8 (\pm 1.3)$	-90 (± 5)	2
	PE19-YAN-C145A	shallow, nearshore	micrite sediment	10.8303	76.0209	12.6	14.2	2	2	$-0.89 (\pm 0.02)$	$19.31 (\pm 0.10)$	$0.640 (\pm 0.004)$	14 (± 5)	$-11.3 (\pm 1.0)$	$-84 (\pm 10)$	7
Tunin	PE19-JUN-C163	shallow, nearshore	micrite sediment	11.0454	75.9973	13.7	24.1	3	-	$-2.42 (\pm 0.01)$	19.95 (± 0.03)	$0.664 (\pm 0.014)$	(9 ∓) ∠	-12.1 (± 1.2)	-87	6
	PE19-JUN-C094	shallow, nearshore	micrite sediment	11.0582	76.1556	1	,	,	-	,	16.98 ^C		,	,	-67	28
												Average (1 σ SD) 13 (\pm 3)	13 (± 3)	-11.7 (± 1.3)	-78 (± 9)	14 (± 9)
	PE19-MEH-Br131A		whole rock bedrock	11.2623	76.0404	1		2		$-2.17 (\pm 0.03)$	$25.32 (\pm 0.01)$	$0.505 (\pm 0.004)$	$61 (\pm 2)$		1	1
Bedrock	PE19-MEH-Br131B	,	whole rock bedrock	11.2623	76.0404	1	,	2	,	$-2.34 (\pm 0.01)$	$25.15 (\pm 0.02)$	$0.513 (\pm 0.015)$	58 (± 6)	,	1	ı
	DF10-DITM-B-073A		whole rock hedrock	10 7206	76.0516			,		134 (+001)	23 51 (+0.05)	0.406 (+ 0.01)	(5 +) 59			

ements were collected opportunistically in the field and do not represent average conditions

Data derived from $\Delta^{1/7}$ O analysis as sample was not analyzed for Δ_{47} .

Declarive to the carbon dioxide equilibrium scale (CDES) of Dennis et al., (2011); the ¹⁷O-correction uses "Brand parameters," (e.g. Petersen et al., 2019), See Table S10.

E Columbiat from Decision and 17017 En. 23.

880

881

882

Table 3. Summary of water isotope data from the Lake Junin region

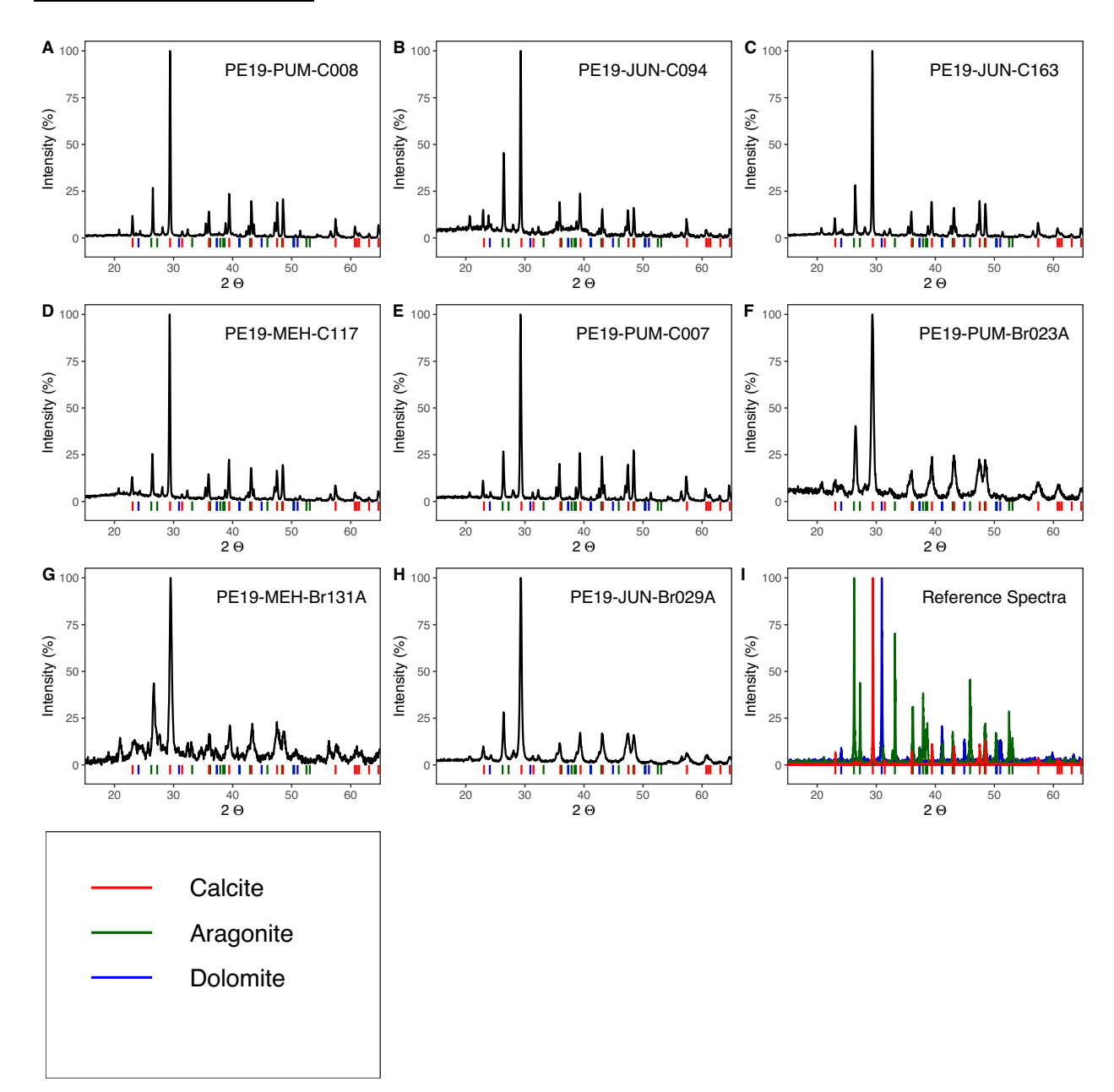
Table 3. Summary of water isotope data from the Lake Junin Region

Sample ID	A	Water Type	No. replicate	d-excess	δ' ¹⁷ O ^B (‰)		δ' ¹⁸ O ^B (‰)		Δ' ¹⁷ O ^B (per meg)	
Sample 1D	Location		Δ' ¹⁷ Ο analyses	(‰)	average	1 σ sd	average	1 σ sd	average	1 σ sd
J1 (6/15/2016)	Junín	precipitation	1	9.39	-11.175		-21.187		12	
J3 (10/15/2016)	Junín	precipitation	2	19.02	-3.493	0.173	-6.681	0.316	35	6
J6 (1/15/2017)	Junín	precipitation	4	11.15	-11.131	0.129	-21.163	0.253	43	9
J7 (2/15/2017)	Junín	precipitation	2	9.05	-10.924	0.108	-20.753	0.197	34	4
J8 (4/15/2017)	Junín	precipitation	2	12.28	-5.803	0.082	-11.042	0.151	27	2
PE19-PUM-P019	Pumacocha	precipitation	2	13.52	-7.906	0.286	-15.016	0.570	22	15
PE19-CAR-S028	Lake Junín	inflow stream	2	5.71	-7.845	0.019	-14.903	0.020	24	8
PE19-JUN-R063	Lake Junín	outflow	5	-6.44	-5.448	0.104	-10.346	0.203	14	12
PE16-JUN-L016	Lake Junín	lake	2	-15.77	-2.202	0.029	-4.159	0.059	-6	2
PE19-JUN-L090	Lake Junín	lake	2	-0.96	-6.483	0.112	-12.326	0.219	25	4
PE19-JUN-L159	Lake Junín	lake	3	-5.04	-5.833	0.296	-11.077	0.566	16	4
PE16-JUN-S027	Lake Junín	isolated pool	2	-35.30	0.961	0.163	1.873	0.323	-28	7
PE16-JUN-S038	Lake Junín	river/stream	2	5.10	-7.519	0.190	-14.277	0.349	19	6
PE16-JUN-S048	Lake Junín	river/stream	2	-0.20	-6.791	0.105	-12.896	0.183	19	8
PE16-JUN-S053	Lake Junín	river/stream	2	-0.76	-6.686	0.121	-12.681	0.234	9	3
PE16-JUN-S019	Lake Junín	spring	1	7.51	-7.445		-14.146		25	
PE19-MEH-L116	Mehcocha	lake	4	3.98	-6.990	0.133	-13.289	0.234	27	14
PE19-PUM-L018	Pumacocha	lake	1	5.07	-6.864		-13.067		36	
PE19-PUM-S016	Pumacocha	outflow	1	5.31	-7.599		-14.435		23	
PE19-YAN-L141	Yanacocha	upper lake	2	-1.27	-6.195	0.009	-11.780	0.025	25	4
PE19-YAN-L155	Yanacocha	lower lake	2	-8.69	-5.097	0.026	-9.673	0.048	10	0
PE19-YAN-S140	Yanacocha	outflow	2	-9.28	-4.725	0.016	-8.951	0.031	1	1

A Sample latitudes and longitudes are given for the Junin precipitation station and surface waters in Tables S1 and S2, respectively.

^B Data generated from triple oxygen isotope analysis and reported on the VSMOW-SLAP scale (Schoenemann et al. 2013).

Supplementary Figures:



885	Figure S1. XRD spectra for lake carbonates (A-E) and bedrock carbonates (F-H) from the Lake
886	Junı́n region. Samples were analyzed at a 2 Θ range from 15 to 65° at a 0.05° resolution. Plotted
887	spectra are blank-corrected and normalized by maximum intensity for each sample. The
888	carbonate mineralogy of each sample is entirely calcite based on comparison to reference spectra
889	(I) for calcite (red; Graf, 1961), aragonite (green; De Villiers, 1971), and dolomite (blue; Antao
890	et al., 2004). Vertical ticks along the x-axis in each plot indicate 2 Θ peaks for calcite (red),
891	aragonite (green), and dolomite (blue).
892	
893	Antao, S.M., Mulder, W.H., Hassan, I., Crichton, W.A., and Parise, J.B., 2004, Cation disorder
894	in dolomite, $CaMg(CO_3)_2$, and its influences on the aragonite + magnesite \Leftrightarrow dolomite
895	reaction boundary: The American Mineralogist, v. 89, p. 1142-1147, doi:10.2138/am-2004-
896	0728.
897	De Villiers, J.P.R., 1971, Crystal Structures of Aragonite, Strontianite, and Witherite: The
898	American Mineralogist, v. 56, p. 758–767.
899	Graf, D.L., 1961, Crystallographic Tables for the Rhombohedral Carbonates: The American
900	Mineralogist, v. 46, p. 1283–1326.
901	

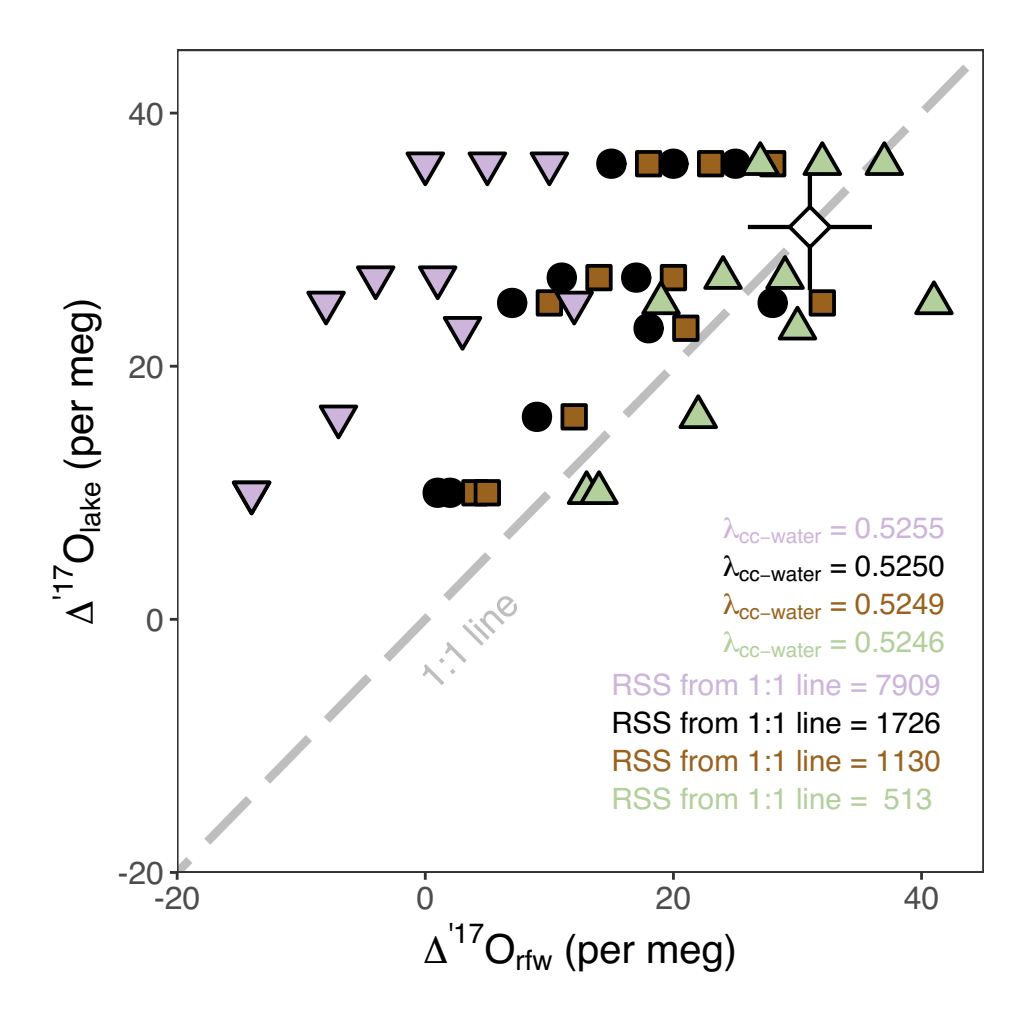


Figure S2. As in Figure 5D, $\Delta'^{17}O$ values of carbonate formation waters ($\Delta'^{17}O_{rfw}$) versus lake water $\Delta'^{17}O$ ($\Delta'^{17}O_{lake}$) values from waters collected at the same sampling locations. Calculated $\Delta'^{17}O_{rfw}$ is shown for four different $\lambda_{calcite-water}$ values: 0.5255 (purple, Wostbrock et al. 2020, GCA), 0.5250 (black, Huth et al., 2022), 0.5249 (brown, Kelson et al., 2022), and 0.5246 (green, greatest parity between $\Delta'^{17}O_{rfw}$ and $\Delta'^{17}O_{lake}$ values). RSS: residual sum of squares.

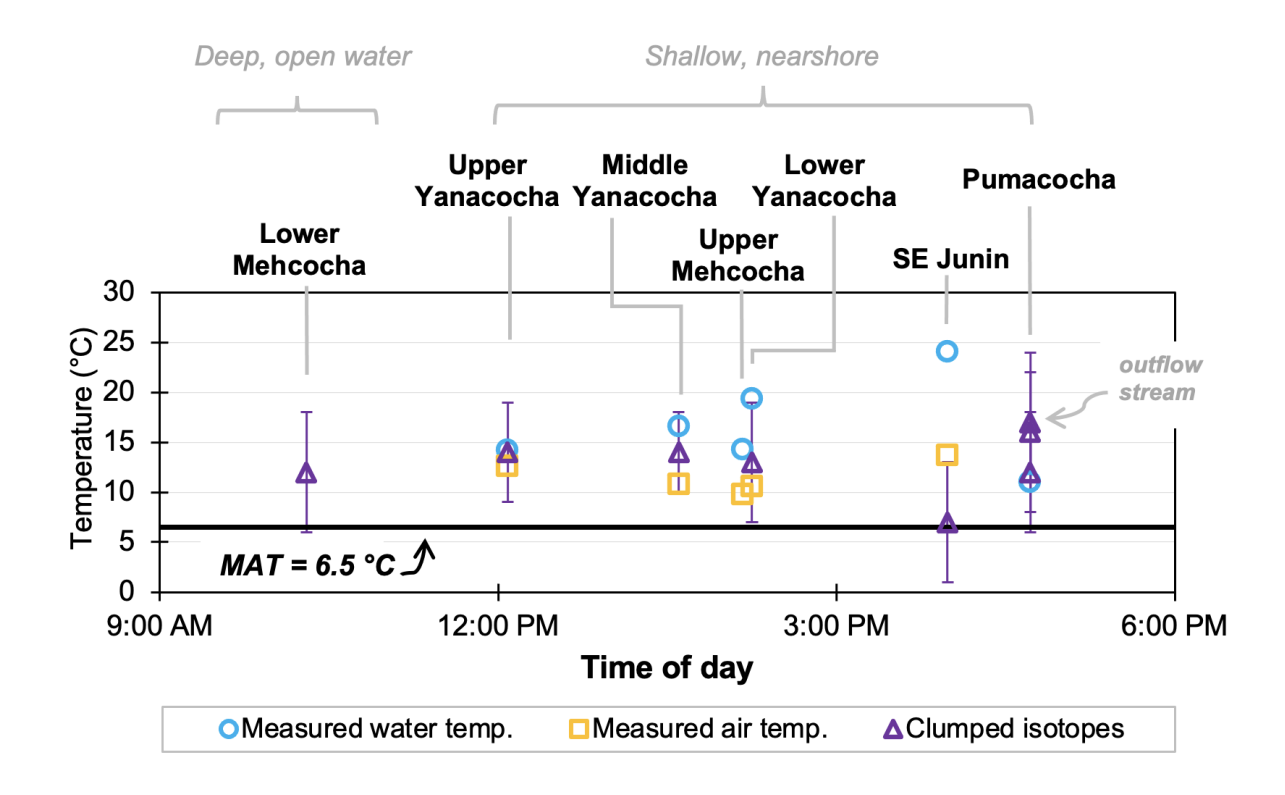
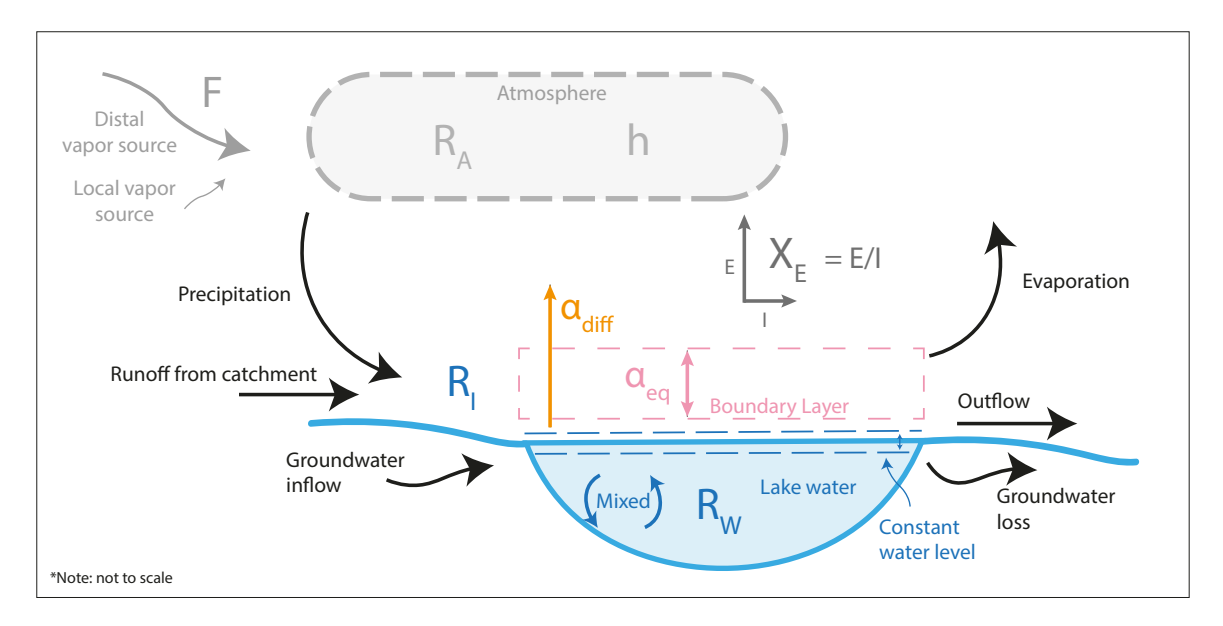


Figure S3. Measured air and water temperatures and clumped isotope temperatures plotted versus time of collection. Note that carbonate samples, and air and water temperature measurements were collected over multiple field days from May 5–10, 2019.



$$R_W = \frac{\alpha_{eq} R_I [\alpha_{diff}(1-h) + h(1-F)] + \alpha_{eq} h X_E R_A F}{X_E + \alpha_{eq}(1-X_E) [\alpha_{diff}(1-h) + h(1-F)]}$$

R_A	Isotopic ratio of atmospheric water vapor.
$R_{_{\rm I}}$	Isotopic ratio of unevaporated input waters.
h	Relative humidity normalized to lake surface temperature.
F	Fraction of local vapor derived from non-lake water sources.
$\alpha_{ m eq}$	Equilibrium fractionation factor between liquid water and water vapor.
$\alpha_{ m diff}$	Kinetic fractionation factor between liquid water and water vapor (relative proportion of diffusive versus turbulent transport).
X _E	Proportion of evaporative losses to inputs (E/I or X_E).

Figure S4. Schematic lake balance diagram of an evaporated, flowthrough lake (after Gibson et al., 2016). Black arrows represent volumetric fluxes. Precipitation, runoff, and groundwater inflow are assumed to be relatively unevaporated with respect to lake water. Note that evaporated lake waters that are returned to the atmosphere may affect both over lake humidity (h) and the isotopic composition of atmospheric water vapor (R_A), though this is not explicitly accounted for in Equation 8. The steady state isotopic lake balance equation (Eq. 8) is included below along with a description of each parameter of the equation (see Table S15 for additional details). Note: not to scale.

Gibson, J.J., Birks, S.J., and Yi, Y., 2016, Stable isotope mass balance of lakes: A contemporary perspective: Quaternary Science Reviews, v. 131, p. 316–328, doi:10.1016/j.quascirev.2015.04.013.

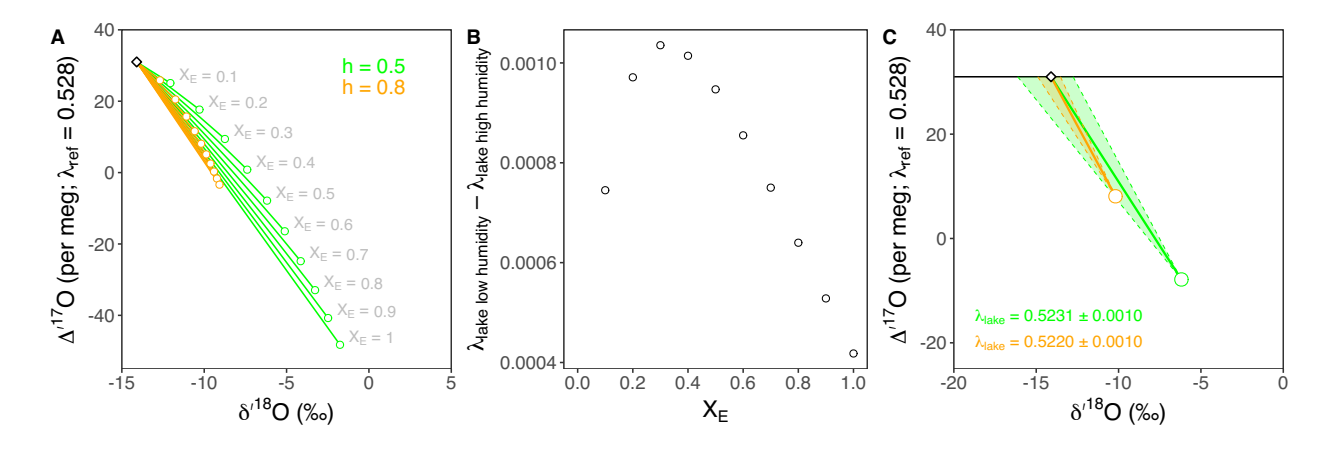


Figure S5. (A) Modeled results using Equation 8 and the following model conditions: Φ = 0.5; F= 0.9; $\delta'^{18}O_I$ = -14.1‰; $\delta'^{18}O_A$ = -25.3‰; $\Delta'^{17}O_I$ = 31 per meg; $\Delta'^{17}O_A$ = 25 per meg; temperature = 14 °C. The model was run over an X_E range from 0.1 to 1.0 (at intervals of 0.1) for h= 0.5 (arid, green) and h= 0.8 (humid, orange). The white diamond represents the composition of unevaporated input waters. Grey labels indicate X_E for the h= 0.5 scenario; labels are not shown for h= 0.8 for clarity, but follow the same trend as for h= 0.5 (i.e., decreasing $\Delta'^{17}O$ with increasing X_E). Note that the solid lines between each model solution and unevaporated input water are equivalent to λ_{lake} in $\delta'^{17}O$ - $\delta'^{18}O$ space and do not represent evaporation trajectories. (B) Difference in λ_{lake} for the two humidity scenarios is shown along the y-axis, versus X_E . The difference in modeled λ_{lake} is highest at relatively low X_E (e.g., 0.2–0.5). (C) As in (A), but showing only the model solutions for X_E = 0.5 at h= 0.5 and 0.8 (green and orange open circles, respectively). Solid colored lines show modeled λ_{lake} for each humidity scenario. Dashed colored

lines show λ_{lake} values ± 0.0010 to illustrate the effect of λ_{lake} uncertainty on $\delta'^{18}O_{rucp}$. Though the magnitude of λ_{lake} uncertainty is the same for both humidity scenarios, the observed effect on $\delta'^{18}O_{rucp}$ is larger in the low humidity scenario (green shading) when $\Delta'^{17}O$ is more distinct from input $\Delta'^{17}O$.

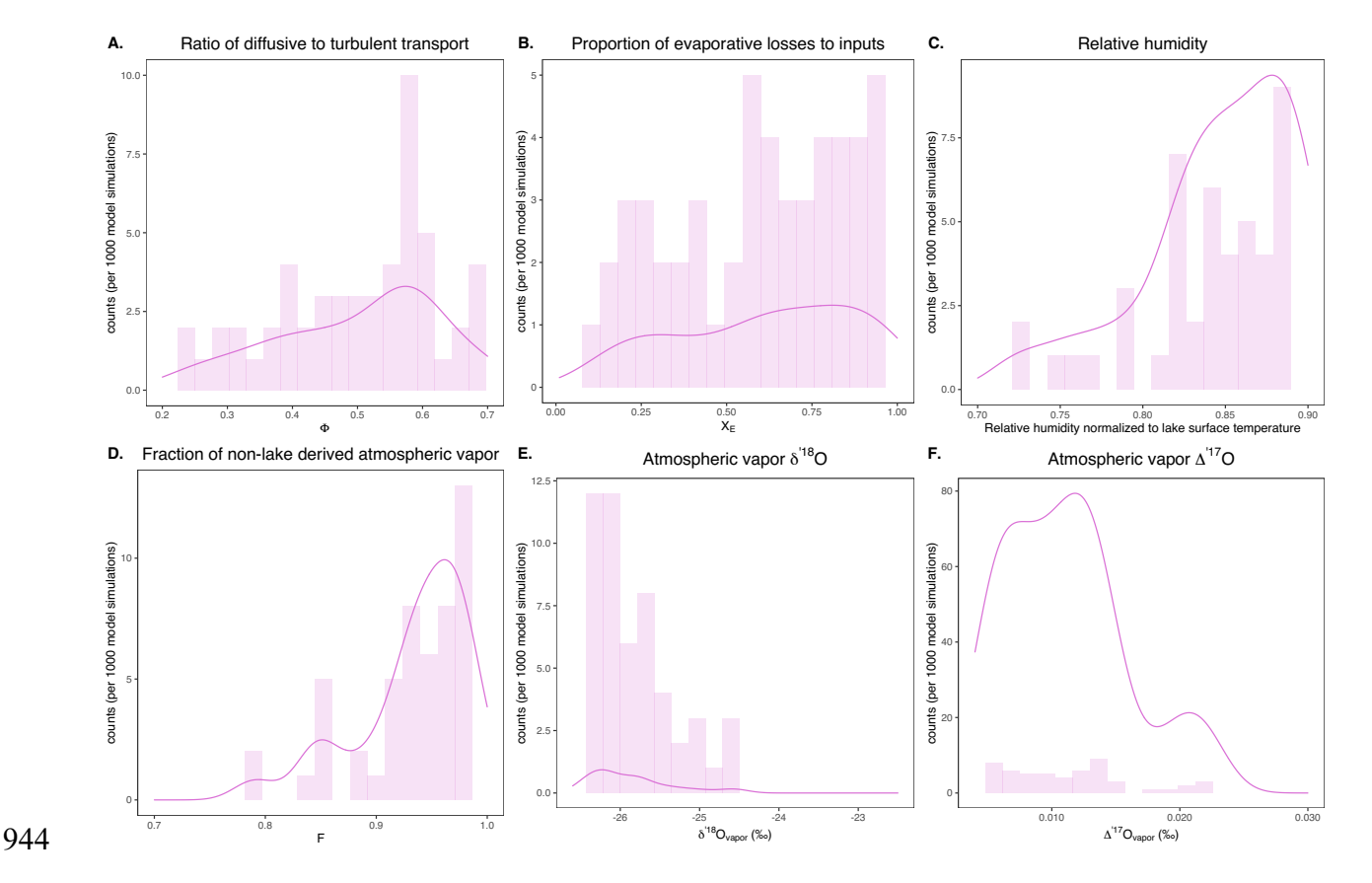


Figure S6. Subset of model solutions shown in Figure 6F for which λ_{lake} <0.5185. Counts for Φ, X_E , h, F, $\delta'^{18}O_{vapor}$, and $\Delta'^{17}O_{vapor}$ are plotted as histograms; probability density functions are shown as solid lines.

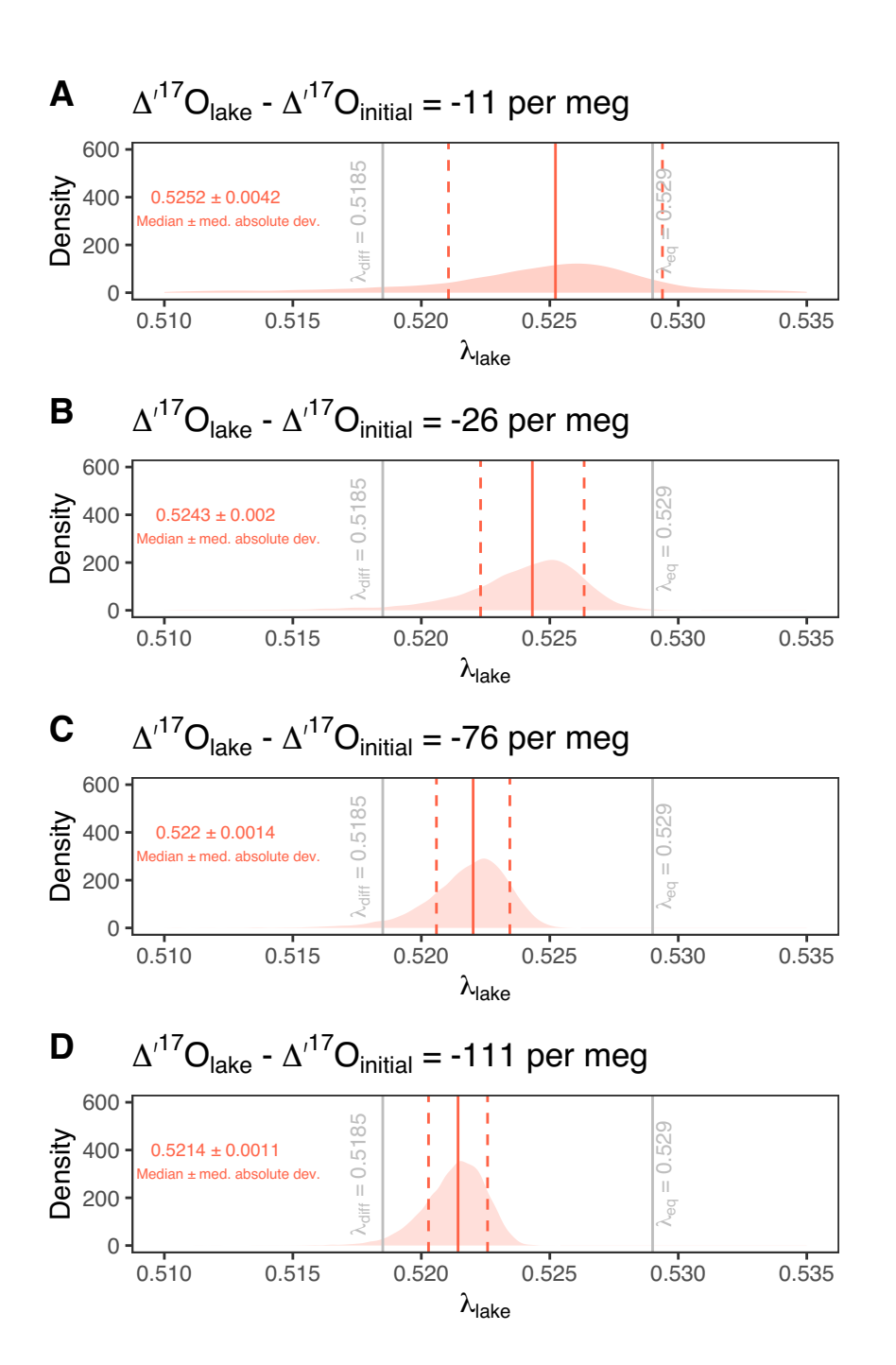


Figure S7. Probability density functions illustrating the propagated error for λ_{lake} based on Monte Carlo resampling (n= 10,000) using uncertainty in carbonate $\Delta'^{17}O_{rfw}$ (10 per meg) and $\delta'^{18}O_{rfw}$ (0.957‰), and precipitation $\Delta'^{17}O$ (5 per meg) and $\delta'^{18}O$ (2.2‰). Panels illustrate the

953	dependency of calculated λ_{lake} uncertainty on the magnitude that lake waters have evolved away
954	from input precipitation.
955	
956	Supplementary Tables:
957	Table S1. Meteorological data, hydrogen and oxygen isotopes of precipitation samples from
958	Junín, Peru
959	Table S2. Surface water hydrogen and oxygen isotope data from the Lake Junín region
960	Table S3. Raw X-ray diffraction data for lacustrine and bedrock carbonates in the Lake Junín
961	region
962	Table S4. Reactor 6 triple oxygen data
963	Table S5. Reactor 8 triple oxygen data
964	Table S6. Reactor 9 triple oxygen data
965	Table S7. Reactor 10 triple oxygen data
966	Table S8. Summarized Reactor 6, 8, 9, and 10 standards
967	Table S9. Pooled standard deviation calculations for Δ^{17} O and Δ_{47}
968	Table S10. Clumped isotope (Δ_{47}) data for gases, carbonate standards, and samples
969	Table S11. Table of regressions for $\delta'^{18}O - \delta'^{17}O$ in water datasets
970	Table S12. Observed λ_{lake} values from the Lake Junı́n region and compiled from literature
971	Table S13. Carbonate formation water Δ^{17} O calculations from Lake Junín region lacustrine
972	carbonates
973	Table S14. Calculated $\Delta'^{17}O_{rfw}$ using published values of $\lambda_{calcite-water}$
974	Table S15. Description of parameters and values used in steady state lake balance equations

975	Table S16. δ^{118} O _{rucp} calculations for Lake Junín Region lake waters, outflow rivers, and
976	lacustrine carbonates using modeled λ_{lake} for different humidity conditions
977	
978	Supplemental R Scripts:
979	Supplemental Script 1: Error propagation for $\delta^{18}O$ values of carbonate formation waters
980	$(\delta^{18}O_{rfw})$ from carbonate $\delta^{18}O_{carb}$ and Δ_{47} values
981	Supplemental Script 2: Lake isotope mass balance model
982	